

Loan copy

Return to:



REPORT No. 33

RC Deane Jr

Errors

pg 2

16

17

9-3

Table 1

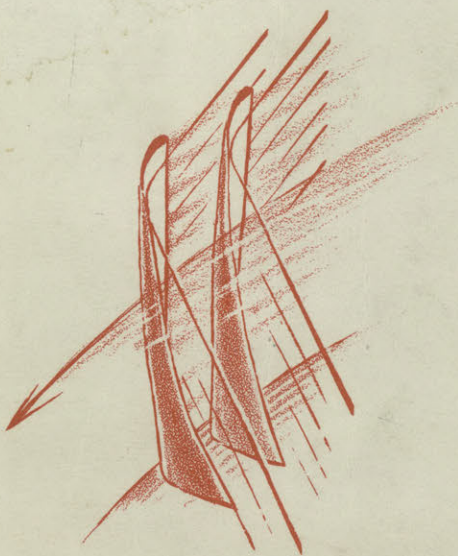
fig 17

A STUDY OF THE END WALL BOUNDARY LAYER IN AN AXIAL COMPRESSOR BLADE ROW

RAYMOND W. MOORE, JR.

DAVID L. RICHARDSON

October 1955



GAS TURBINE LABORATORY
MASSACHUSETTS INSTITUTE OF TECHNOLOGY
CAMBRIDGE · 39 · MASSACHUSETTS

SHEAR FLOW IN BENDS

A STUDY OF THE END WALL BOUNDARY LAYER
IN AN
AXIAL COMPRESSOR BLADE ROW

Raymond W. Moore, Jr.
David L. Richardson

Under the sponsorship of:
Office of Naval Research
Contract N5ori 07848

Gas Turbine Laboratory
Report Number 33
October 1955

Massachusetts Institute of Technology

ABSTRACT

Turbulent end wall boundary layers in the hub region of axial compressor blade rows have been studied in the Gas Turbine Laboratory. Both analytical and experimental work are presented. An attempt was made to predict the growth of the boundary layer momentum thickness as it passes through a cascade of blades using the momentum integral equation and several assumptions. This calculation was compared with measurements taken along an assumed free streamline in a stationary cascade of blades supplied with an artificially skewed inlet boundary layer. From this comparison, the relative influence of individual terms in the momentum integral equation is deduced. The effects of inlet skewing and cross flow in the boundary layer in the region between blades is described. Two methods of representing main and cross flow velocity profiles are compared with experimental data.

TABLE OF CONTENTS

	<u>Page No.</u>
Abstract	
Table of Contents	
List of Symbols	
1 Introduction	1
2 Description of Flow in the Hub Region	1
3 The Investigation	3
3.1 General Approach and Some Assumptions	3
3.2 Some Observations in a Cascade of Compressor Blades	4
3.2.1 Simulation of Flow in Compressor Blade Row in a Rectilinear Cascade	4
3.2.2 Blade Geometry, Free Stream Properties and Inlet Conditions	4
3.2.3 Boundary-Layer Flow Through Blades and Exit Conditions	6
3.2.4 Blade Forces	6
3.3 Calculation of θ_x Along Assumed Streamline Axis	6
4 Discussion of Results	7
4.1 Qualitative Description of the Boundary Layer Flow Along the Assumed Streamline Axis	7
4.2 Limitations in Calculating the Boundary Layer Flow	8
4.3 Variations of the Boundary Layer Flow in the Tangential Direction	9
4.4 Comparison of the Present Case to Cascade Results Made with a Uni-Directional Inlet Flow	10
5 Conclusions	11
5.1 Effects of Inlet Skewing and Cross Flow in the Boundary Layer in the Region Between the Blades	11
5.2 Designs to Accommodate Wall Boundary Layer Flow	11
5.3 Information Required for Further Analysis	11
Bibliography	12

Appendices

A.1 Description of Cascade and Instrumentation	13
B.1 Theory of Turbulent Boundary Layer With Cross Flow	14
B.1.1 Momentum Integral Equations	14
B.1.2 Velocity Profiles	15
B.1.3 Shear Stress Law	19
B.1.4 Possible Solutions	19
Tables and Figures	20

LIST OF SYMBOLS

X	axial direction	
Z	tangential direction	
x, y, z	curvilinear coordinates (see definition Section 3.1)	
u, v, w	velocity components in the boundary layer along x, y and z coordinates	
V	velocity vector within the boundary layer	
U	free stream velocity just outside of the boundary layer	
s	pitch	
c	chord	
p	static pressure	
p ₀	stagnation pressure	
q	dynamic head $q = p_0 - p$	
H	shape factor $H = \frac{\delta^*_x}{\theta_x}$	
r	empirical exponent Equation (18)	
m, n	empirical exponents defined by Mager ¹	
δ	boundary layer thickness	
θ_x, δ^*_x θ_z, δ^*_z θ_{xz}	} boundary layer integral quantities defined in Appendix B	
β		air angle
ξ		stagger angle
i	incidence	
θ	camber angle	
$r\Omega$	wheel speed	
C _p	cascade static pressure rise coefficient $C_p = \frac{p_2 - p_1}{(p_0 - p)_1}$	

SUBSCRIPTS

x, y refer to coordinate axes

SUPERSCRIPTS

' primes denote quantities relative to moving blades

1 Introduction

The flow near the casing of axial compressors is difficult to predict since viscous forces are appreciable. If the flow near the wall at the exit of a row of blades could be calculated, given the inlet flow conditions, the blade geometry and the end wall configuration, single-stage and multi-stage compressor performance could be more reliably estimated. The problem can be considered as one of the boundary layer type, the turbulent case being most important for compressors. A study directed toward the solution of the problem has been conducted in the M.I.T. Gas Turbine Laboratory. Some interesting results, mostly of a qualitative nature, have come from the work and are reported in this paper.

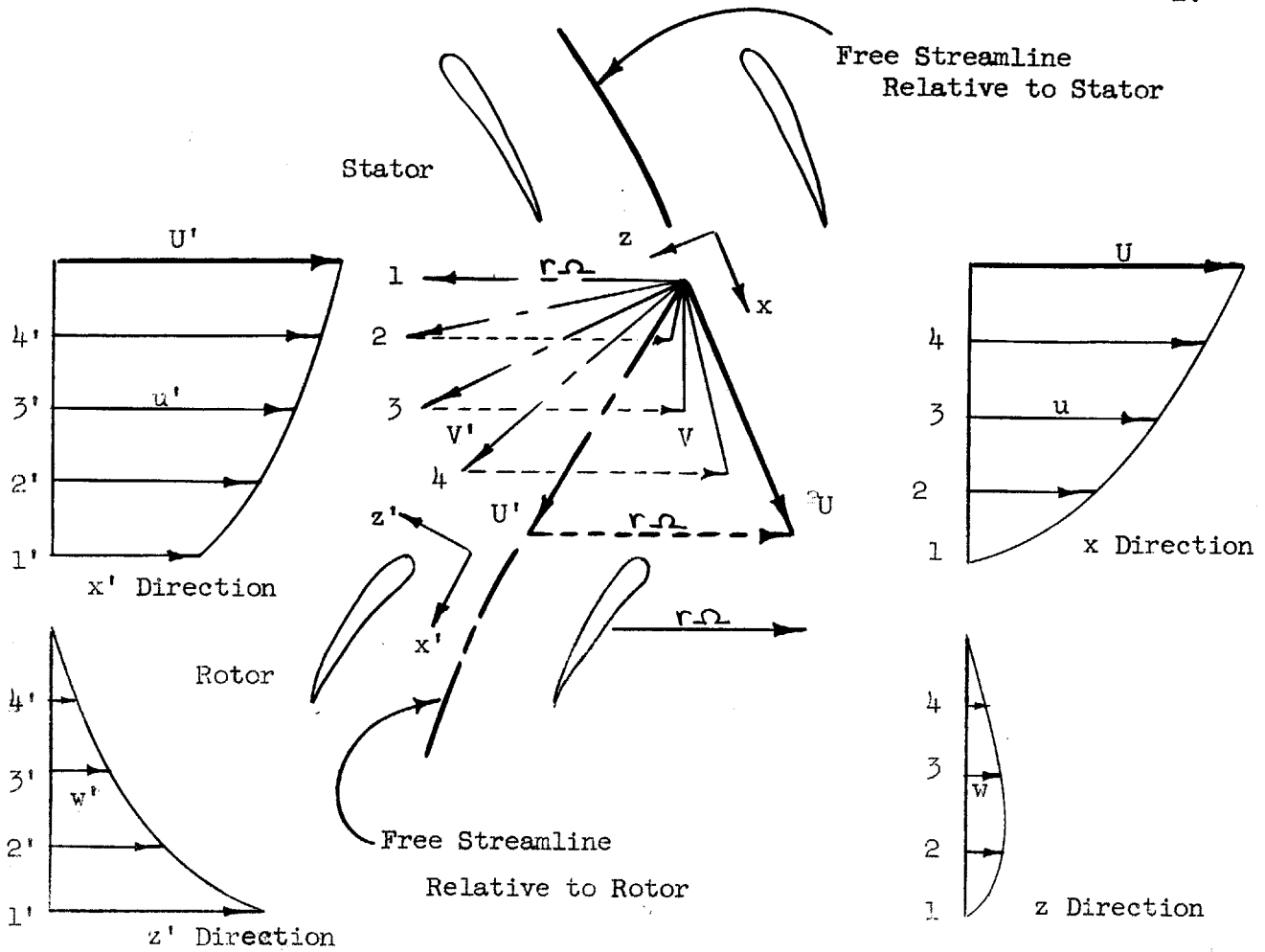
2 Description of Flow in the Hub Region

The blade configuration at the casing; i.e. clearance between the tips of the blades and the wall and any motion of the casing relative to the blades, strongly influences the character of the problem. Since the inlet flow to a given row is determined by the previous row, the configurations of the boundaries in two successive rows must be specified for any particular problem. We have limited our investigation to one overall configuration of an axial compressor blade row where:

1. No clearance exists between the blade tip and the casing.
2. The casing, or end wall, is stationary with respect to the blades.
3. The previous row has the same configuration.

This overall configuration would be found at the hub of a compressor with shrouded stator roots as shown in Figure 1.

Consider the flow at Section A-A, Figure 1. The velocity triangles at that point might be as shown below.



Velocity Profiles in x' and z' Directions Relative to the Rotor

Velocity Profiles in x and z Directions Relative to the Rotor

Primes denote quantities relative to rotor.

STATOR

By addition of the wheel speed vector ($r\Omega$) to flow relative to the stator one gets the flow relative to the rotor. It is interesting to notice how a boundary layer which is essentially unidirectional (such as the one shown leaving the stator above) can become highly skewed relative to the rotor by adding the wheel speed vector. In the above figure, U refers to the exit velocity from the stator and U' to the entrance velocity to the rotor, both at some distance away from the casing, while V and V' denote the same velocities at some point in the

boundary layer near the inner casing. The flow entering the rotor blade row near the wall (i.e. the entering boundary layer) has a high angle of incidence on the blades (which, we assume, have been designed to accept the free stream angle) and, unlike conventional boundary layers, has kinetic energy comparable to the free stream. The velocity varies from $r\Omega$, the wheel speed directed tangentially, at the rotor hub to U' , directed at some design angle (in the neighborhood of 40° or 50° , measured from the axial direction) at some distance away from the wall.

As the boundary layer fluid flows on to the rotor, high shear stresses near the wall (Figure 1) dissipate some of its kinetic energy. The boundary layer fluid progresses through the blade row, acted upon by pressure forces and viscous forces, with changing velocity and direction. The pressure field tends to accelerate any velocity deficient fluid toward the suction side of the blade passage and a flow as shown in Figure 2 is common.

The same events occur as the fluid progresses through the succeeding stator.

3 The Investigation

3.1 General Approach and Some Assumptions

The discussion will be limited to an incompressible fluid. We consider the flow relative to the blades and will refer to the flow outside the boundary layer as the free stream. The change in the radius, measured from the axis of the machine to a free streamline, will be assumed small so that the stagnation pressure based on the relative velocity, $p + \frac{\rho U^2}{2}$, will be constant along a free streamline. The region of shear flow near the casing will be considered a proper boundary layer, with small thickness, which is turbulent.

It is convenient to think in terms of a curvilinear coordinate system where the x-axis is in the direction of the free stream just outside the boundary layer, the y-axis is perpendicular to the end wall or casing and the z-axis is perpendicular to the x and y axes so as to form a right hand, orthogonal system. The velocity of the free stream, just outside the boundary layer is U and the velocity components in the boundary layer along the x, y and z axes are u , v and w respectively. w is often called the "cross flow" velocity.

The blades will determine the flow field just outside the boundary layer and since we are primarily concerned with the boundary layer flow, we assume the velocity, static pressure and curvature at each point of every free streamline are known. For thin boundary layers, $\frac{\partial p}{\partial y} \approx 0$ and the pressure through the boundary layer is determined by the free stream.

A complete solution of the problem would yield the velocity and direction of flow within the boundary layer over a region between two blades such as the one in Figure 2. This information could also be presented in terms of the boundary layer flow along several different x-axes, each being a different free streamline. In our study, attention has been focused on just one free streamline, the one which leaves the blade row approximately halfway between two blades, Figure 2.

3.2 Some Observations in a Cascade of Compressor Blades

3.2.1 Simulation of Flow in Compressor Blade Row in a Rectilinear Cascade

Studying the behavior of the wall boundary layer in an actual machine is quite difficult for several reasons. Measurements relative to the blades at inlet, between the blades and at outlet are necessary. In a rotor such measurements involve considerable mechanical complication. In a stator following a rotor, fluctuations of the flow with time are present. In addition, the dimensions of the flow passage between blades in a machine are generally too small to permit accurate measurements.

To avoid these difficulties, a cascade was constructed* to simulate the flow near the hub of an axial compressor rotor. An axial entry rotor was simulated to simplify future comparisons with measurements in an actual machine. (Some measurements have been made in an axial entry rotor but no comparisons have yet been possible.)

The axial entry rotor meets the conditions described in Section 2. and contains the important features of hub flow, the skewness and relatively high kinetic energy of the boundary layer at the blade row entrance.

The testing of a cascade with skewed, high kinetic energy inlet flow near the wall poses several new problems so the initial investigation was exploratory and made use of available equipment. As a result, the accuracy of measurements (particularly flow direction) was not very good. The apparatus and measuring techniques are described in Appendix A.

3.2.2 Blade Geometry, Free Stream Properties and Inlet Conditions

The airfoils had:

Circular arc camber line
NACA Four Digit Series thickness distribution with 9%
maximum thickness

* The construction and testing of the cascade were the subjects of an S.M. Thesis in the Gas Turbine Laboratory, Reference 5.

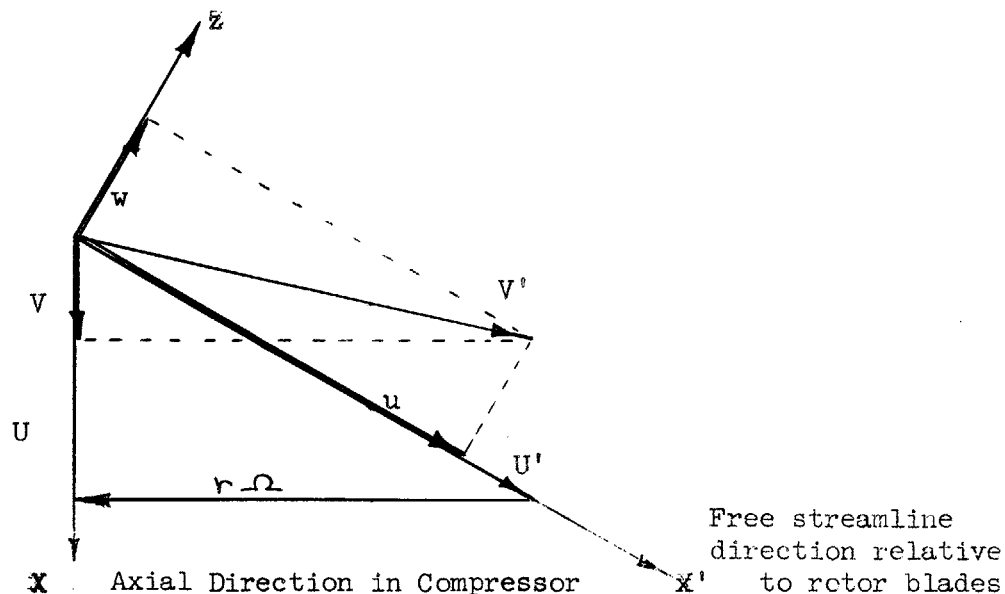
Chord, $C = 2.8''$
 Camber angle, $\theta = 35^\circ$

The cascade was set within:

Stagger angle, $\xi = 34.3^\circ$
 Pitch-chord ratio, $s/c = 0.828$

The free stream flow entered at $\beta_1 = 52^\circ$ and left at $\beta_2 = 22.5^\circ$ (angles measured as shown in Figure 3). The resulting distribution of static pressure at the wall is shown in Figure 4. The distribution of dynamic head, q ($q \equiv p_0 - p$), along the axis shown in Figure 4 (assumed to be a free streamline) is plotted in Figure 5. The points B, E, G, H, I and J_2 refer to measuring stations along the center streamline as shown in Figure 6. The overall static pressure rise coefficient, C_p , for the free stream was $C_p = 0.337$.*

The inlet conditions to the axial entry rotor were measured in the machine, then approximated in the cascade. The inlet velocity, V , relative to the stationary hub is plotted versus y , the distance from the hub, in Figure 7. It should be noted that in this case the boundary layer relative to the stationary hub was not skewed and in the axial direction. To get the flow in the streamline coordinate system relative to the moving blades, a vector addition of the wheel speed to the air velocity relative to the casing was performed at each value of y . The relative velocity was reduced to its components u and w , as shown in the diagram.



* This value differs from the value predicted by two-dimensional theory because the cascade did not behave uniformly. One of the five blade passages was badly stalled over its entire span.

where: U is velocity relative to the casing outside the boundary layer
 V is velocity relative to the casing at a point within boundary layer
 U' is the velocity relative to the moving blades at $y = \delta$
 V' is the velocity relative to the moving blades within the boundary layer
 x and z are streamline coordinates relative to the blades
 u and w are velocity components in the x and z directions
 $\frac{U}{r\Omega} = 1.073$ for the case simulated.

The resulting inlet velocity profiles are plotted in Figure 8 along with the cascade approximations.

3.2.3 Boundary Layer Flow Through Blades and Exit Conditions

The u and w velocity profiles were measured* at points A, B, C, D, E, F, G, H, I, J₁, J₂, J₃ along the bottom wall of the cascade, Figure 6, and the results are presented in Figures 10 and 11. The progress of the boundary layer flow along the free streamline axis can be observed from the measurements at B, E, G, H, I and J₂. Some idea of flow variations across the passage can be obtained from the other profiles. The integral quantities appearing in the momentum integral equations ** have been calculated from the velocity profiles and are tabulated in Table I.

The bottom wall of the cascade was coated with a mixture of kerosene and carbon black before one of the runs. When the flow was turned on, traces were made on the coating which are roughly indicative of the flow direction adjacent to the wall. Figure 12 is a photograph of the resulting traces.

3.2.4 Blade Forces

The static pressure distribution around the blades was measured at several distances, Y, from the end wall. The axial and tangential components of the pressure force on the blade were computed and are plotted vs. Y in Figure 13. The forces are normalized with the value at Y = 1.5 inches, which was taken to be the free stream condition.

3.3 Calculation of θ_x Along Assumed Streamline Axis ***

The momentum integral equation along a free streamline axis is:

$$\frac{\partial \theta_x}{\partial x} + \frac{\theta_x}{\delta} \frac{\partial \delta}{\partial x} \left(\frac{H+2}{2} \right) + \frac{\partial \theta_{xz}}{\partial z} = \frac{\tau_{ox}}{\rho g} \quad (1)$$

* Measuring techniques are described in Appendix A.

** See Appendix B for momentum integral equations.

*** For a discussion of calculation methods, see Appendix B.

Mager (Reference 1) was able to calculate the growth of θ_x along a free streamline axis in a 90° bend by neglecting the term contributed by the presence of cross flow, $\frac{\partial \theta_{xz}}{\partial z}$. Using this assumption for the present case, the variation of θ_x along the assumed streamline was calculated with:

1. The measured variation of q with x , Figure 5.
2. $H = 1.30$, an average value suggested by the data.
3. The Squire and Young formula for skin friction as presented in Reference 3,

$$\frac{2\tau}{\tau_{0x}} = \left[5.89 \log_{10} (4.075 R_\theta) \right]^2$$

4. The initial θ_x from the data at point E, $\theta_{xE} = 0.0437$ inches.

The calculations were started at point E and carried to point J₂; no attempt was made to include the high shear region from B to E. The result of the calculation is plotted in Figure 14.

4 Discussion of Results

4.1 Qualitative Description of the Boundary Layer Flow Along the Assumed Streamline Axis

At the leading edge of the splitter plate the velocity is high and is directed parallel to the plane of the cascade. (Simulating the flow on to the rotor hub where the velocity adjacent to the rotor hub is ωr directed tangentially.) This velocity is immediately reduced to zero and the velocities near the wall quickly decreased in a region of high shear stress from B to E, Figure 6. This shearing action, combined with the decelerations caused by the pressure field, causes a decrease in the z component of velocity, w , and an increase in the u component near the wall from B to E. As a result, the angle between the streamline at the wall and the free stream goes from 24.5° at B to 10.0° at E. This pronounced turning near the wall is indicated by the carbon black traces, Figure 12. It is interesting to note that in this region θ_x is decreasing in the x direction, though the x pressure gradient is adverse (pressure rising in the x direction),

The component of the pressure gradient in the x direction, is positive, while the gradient in the z direction, $\frac{\partial p}{\partial z}$, is negative at all points from B to J₂. (The orientation of the x and z axes are shown in Figure 2.) The pressure gradient in the z direction decelerates the negative cross flow from B to G to zero at some point between G and H. From H to J₂ the cross flow is positive and is accelerated by the

z pressure gradient. Thus, the boundary layer fluid, which entered the cascade at an angle larger than β_1 , the free stream inlet angle, is overturned and leaves the blading at an angle smaller than β_2 , the free stream exit angle. The process is illustrated in Figure 2.

4.2 Limitations in Calculating the Boundary Layer Flow

A method for writing the momentum integral equations in terms of four variables θ_x , H , ϵ and r is described in Appendix B. The shape factor of the u velocity profile, H , was fairly constant along the assumed streamline axis, but the value of r varied appreciably.

The absence of an expression to relate r to the other variables prevented any attempt at a complete solution. The calculation in Section 3.3 was possible since the omission of the $\frac{\partial \theta_{xz}}{\partial z}$ term and the assumption of some constant value for H resulted in a simple total differential equation with one dependent variable, θ_x .

The variation of θ_x along the assumed streamline, as calculated in Section 3.2.3 is compared with the measured variation in Figure 14.

The calculation predicts considerably more growth in θ_x than the measurements indicate, implying that neglecting the cross flow term, $\frac{\partial \theta_{xz}}{\partial z}$ in Equation (1) is not justified. This implication is strengthened by a look at the measured data. Using the rough approximation that

$$\left(\frac{\partial \theta_{xz}}{\partial z}\right)_E \sim \frac{(\theta_{xz})_E - (\theta_{xz})_C}{z_E - z_C}$$

(where subscripts refer to points in the flow, Figure 6)

we find

$$\left(\frac{\partial \theta_{xz}}{\partial z}\right)_E \approx +0.007$$

The same calculation can be done by interpolating the data for a point upstream of J_2 (about 0.3" upstream along the axis) to give

$$\left(\frac{\partial \theta_{xz}}{\partial z}\right)_{\text{UPSTREAM OF } J_2} \approx +0.006$$

The pressure gradient and shear stress terms at E and J₂ are:

At E

$$\frac{\theta_x}{\delta} \frac{\partial \delta}{\partial x} \left(\frac{H+2}{2} \right) \approx -0.008 \quad (\text{measured})$$

$$\frac{\tau_{ox}}{2\delta} \approx +0.0017 \quad (\text{Calculated as in Section 3.3})$$

At J₂

$$\frac{\theta_x}{\delta} \frac{\partial \delta}{\partial x} \left(\frac{H+2}{2} \right) \approx -0.015 \quad (\text{measured})$$

$$\frac{\tau_{ox}}{2\delta} \approx +0.0015 \quad (\text{Calculated as in Section 3.3})$$

The cross flow term, $\frac{\partial \theta_{xz}}{\partial z}$, is of the same order of magnitude as the other terms contributing to $\frac{\partial \theta_x}{\partial x}$. Further, $\frac{\partial \theta_{xz}}{\partial z}$ is opposite in sign to the pressure gradient term and tends to decrease θ_x . Thus, when the cross flow term was neglected in Equation (1), the calculated growth of θ_x was larger than that which actually occurred.

4.3 Variations of the Boundary Layer Flow in the Tangential Direction

The boundary layer flow along the streamlines, other than the one in the center of the passage, has not been investigated. The pressure field is different along each streamline and near the blades the component of flow perpendicular to the wall no doubt exerts appreciable influence on the boundary layer behavior. To give some idea of the result of the boundary layer flow within the passage, the variation of the integral quantities across the passage at exit are shown in Figures 15 and 16. In Figure 15, the large values of δ_x^* and θ_x near the suction side of the passage indicate the accumulation of low energy fluid in that region as a result of the cross flow.

4.4 Comparison of the Present Case to Cascade Tests Made with a Uni-Directional Inlet Flow

The cascade blades used in this study (described in Section 3.2.2) had been used in previous investigations of three-dimensional flow near the end walls. The tests were run with an inlet flow, including the boundary layer, which was uniform in direction, and the cascade set with:

$$\begin{aligned} \text{Stagger angle, } \xi &= 22.5^\circ \\ \text{Pitch-chord ratio, } s/c &= 1.0 \end{aligned}$$

The free stream entered at $\beta_1 = 40^\circ$ and left at $\beta_2 = 15^\circ$. Measurements included:

Velocity profiles at inlet and exit
Distribution of static pressure over the end wall
Distribution of static pressure around the blades at several distances from the end wall

A free streamline was assumed, and using the measured inlet θ_x , of 0.093 inches and the static pressure variation along the streamline, θ_x at outlet was calculated neglecting the cross flow term, $\frac{\partial \theta_{xz}}{\partial z}$ in the x momentum integral equation, as in Section 3.3. The calculated value is 0.149 inches while the measured value is 0.149. Such agreement is surprising, for the cross flow term, $\frac{\partial \theta_{xz}}{\partial z}$, at the exit plane is of the same order of magnitude as $\left(\frac{H+\Delta}{\Delta}\right) \frac{\theta_x}{q} \frac{\partial q}{\partial x}$, the x pressure gradient term. Apparently, the cross flow term, $\frac{\partial \theta_{xz}}{\partial z}$, which is positive at exit, changes sign somewhere along the center streamline so that its net effect on the growth of θ_x is small. This was not true in the case with a skewed inlet boundary layer flow. This comparison is only qualitative since the blade stagger angles in the cascade and the resulting free stream flow differed for the two cases.

The distribution of axial and tangential components of pressure force on the blades versus y, the distance from the end wall is presented in Figure 17, for the cases with and without inlet skewing. The forces at the wall are higher when skewing is present due to the higher velocities near the wall and the larger angle of incidence on the blades. The forces were normalized on the basis of the free stream.

5 Conclusions

5.1 Effects of Inlet Skewing and Cross Flow in the Boundary Layer in the Region Between the Blades

The relative motion between one blade row and the next row causes the wall boundary layer to be energized and skewed, relative to the next blade row, by the vector addition of the wheel speed. A boundary layer leaving one blade row with large velocity deficiency is energized and gets a "fresh start" as it enters the next row, a very helpful situation in a machine with continuously rising static pressure along the flow path.

The boundary layer flow at inlet is initially at a larger angle with the axial direction than free stream but is overturned and leaves the blade row at a smaller angle than the free stream. The cross flow provides a mechanism whereby the unusually large velocities in the skewed inlet flow near the wall can be diverted and made more coincident with the free stream flow. The resulting blade pressure force near the wall retains a fairly high value. (85-90% of the free stream force.)

5.2 Designs to Accommodate Wall Boundary Layer Flow

The effects described in Section 4.1 might be put to good use. If blades were designed to accept the skewed inlet flows near the casing with small incidence and to turn the flow in a reasonable rising static pressure field, the losses in the region should be reduced. The work done by the blade forces, which are appreciable (Figure 13) would increase the stagnation pressure of the fluid. Blades which are not designed to accept the skewed inlet flows are likely to be stalled near the casing. Losses in the region will be high and little of the work done on the fluid will result in stagnation pressure rise.

5.3 Information Required for Further Analysis

The method for writing the momentum integral equations in the x and z directions in terms of four variables presented in Appendix B must be supplemented by additional information if analytical solutions are to be obtained. The most useful information would be two more expressions relating H and r to θ_x and ϵ . Perhaps a relationship analogous to the Von Doenhoff and Tetervin (Reference 3) expression for H in two-dimensional flow* can be found. Without two more relationships, solutions are only possible when H and r are constant. To know whether or not H and r are constant for a particular case requires considerable a priori knowledge of the flow.

*
$$\theta \frac{dH}{dx} = e^{4.68(H-2.975)} \left[-\frac{\theta}{r} \frac{dr}{dx} \frac{2r}{\tau_0} - 2.035(H-1.286) \right]$$

BIBLIOGRAPHY

1. Mager, Arthur, "Generalization of Boundary-Layer Momentum-Integral Equations to Three-Dimensional Flows Including Those of Rotating Systems", NACA TN 2310, March 1951.
2. Mager, A., Mahoney, John J. and Budinger, Ray E., "Discussion of Boundary-Layer Characteristics Near the Wall of an Axial-Flow Compressor", NACA Report 1085, 1952.
3. Von Doenhoff, Albert E. and Tetervin, Neal, "Determination of General Relations for the Behavior of Turbulent Boundary-Layers", NACA Report 772, 1943.
4. Gruschwitz, E., "Turbulente Reibungsschichten mit Sekundaerstroemung", Ingenieur-Archiv, Vol. VI, 1935, pp. 355-365.
5. Richardson, David L., "The Experimental Investigation of Flow in a Compressor Cascade with a Skewed Inlet Wall Boundary-Layer", M.I.T. Gas Turbine Laboratory, S.M. Thesis, August 1955.
6. Roche, R.F. and Thomas, L.R., Jr., "The Effects of Slotted Blade Tips on the Secondary Flow in a Compressor Cascade", M.I.T. Gas Turbine Laboratory, S.M. Thesis, 1954.
7. Keuthe, A.M., McKee, P.B. and Curry, W.H., "Measurements in the Boundary-Layer of a Yawed Wing", NACA TN 1946, 1949.

APPENDIX A

A.1 Description of Cascade and Instrumentation

The cascade mentioned in the body of this report was designed to approximate flow conditions in the blade passages of an axial compressor rotor. The outstanding features of this cascade were:

1. The end-wall boundary layer entering the plane of the cascade was highly skewed; the flow at the wall being at a high angle of incidence.
2. A moving end wall ahead of the cascade was simulated by use of a flow splitter and a suction slot.

Two techniques were employed together to produce the skewed inlet boundary layer. In the first method, a high velocity jet of air was injected below and at an angle with the main flow. This jet exerts a strong shearing action on the main duct flow and was used to produce a high-velocity cross-flow very close to the wall. The second method of developing cross-flow in the boundary layer was to produce a slight curvature in the main flow upstream of the cascade. The main duct flow was forced to curve by suction and blowing on the side walls of the duct ahead of the cascade.

Simulation of the moving wall ahead of the cascade was accomplished with a sharp flow splitter and a suction slot in the end wall ahead of the cascade blades. This, in effect, allows the velocity adjacent to the wall to remain high. The high velocity jet passing in front of the cascade is split by the sharp leading edge, some flow goes down the suction slot and some goes through the cascade as illustrated in Figure 34. Figure 9 is an overall photograph of the cascade taken through the transparent side of the ducting upstream of the blades. It shows the high velocity jet ducting, the main flow curvature sucking and blowing ducts, the sharp leading edge flow splitter and suction slot and the upstream duct boundary-layer-removal slot.

Traverses were made with a rig equipped with a micrometer for measuring distance from the wall and a protractor for measuring flow direction. Two probes were fitted separately into this rig. The first was a three-hole cobra probe of .014 inch I.D. tubes which measured total pressure and angle. Static pressure was measured with an 1/8 inch O.D. sphere static probe set at the angle found with the cobra probe. Velocities at all measuring positions were calculated from the difference between measured total and static pressures. To measure pressures, probes were attached to a system consisting of a pressure transducer and a galvanometer. Pressure distribution on the blade surfaces were measured with the aid of two blades equipped with static taps, one tapped on the suction surface and the other on the pressure side.

APPENDIX B

B.1 Theory of Turbulent Boundary Layer with Cross Flow

B.1.1 Momentum Integral Equations

Since expressions relating the turbulent shear stresses to the mean flow are not known, exact solution of the boundary layer equations are impossible in the turbulent case. However, the equations, when integrated through the boundary layer, can be used for approximate solutions. Mager (Reference 1) has derived the momentum integral equations in the free streamline coordinate system. When limited to apply only to the flow along the x-axis by setting $z = 0$, the equations in a coordinate system rotating with constant angular velocity, Ω , are:

$$\frac{\partial \theta_x}{\partial x} + \frac{1}{g} \frac{\partial g}{\partial x} \left(\frac{\delta_x^*}{2} + \theta_x \right) + \frac{\partial \theta_{xz}}{\partial z} - 4 \frac{\Omega y}{U} \theta_{xz} = \frac{\tau_{ox}}{2g} \quad (2)$$

$$\frac{\partial \theta_z}{\partial z} + \frac{\partial (\delta_z^* - \theta_{xz})}{\partial x} + \frac{1}{2g} \frac{\partial g}{\partial z} (\theta_z - \theta_x - \delta_x^*) + \frac{1}{g} \frac{\partial g}{\partial x} (\delta_z^* - \theta_{xz}) - 2 \frac{\Omega y}{U} (\theta_x + \theta_z) = - \frac{\tau_{oz}}{2g} \quad (3)$$

The terms involving Ωy are extremely small for many cases and will be excluded.

With the flow along the free streamline just outside the boundary layer specified (i.e. $U, \frac{\partial U}{\partial x}$ and $\frac{\partial U}{\partial z}$), the two equations contain seven

dependent variables, five integral quantities depending on the u and w velocity distributions and two wall shear stresses.

The definitions of the integral quantities are:

$$\delta_x^* \equiv \frac{1}{U} \int_0^d (U - u) dy \quad (4)$$

$$\theta_x \equiv \frac{1}{U^2} \int_0^d (U - u) u dy \quad (5)$$

$$\delta_z^* \equiv \frac{1}{U} \int_0^d w \, dy \quad (6)$$

$$\Theta_z \equiv \frac{1}{U^2} \int_0^d w^2 \, dy \quad (7)$$

$$\Theta_{xz} \equiv \frac{1}{U^2} \int_0^d (U - u) w \, dy \quad (8)$$

Obviously, either the number of variables must be reduced or more equations must be obtained to permit any kind of a solution.

B.1.2 Velocity Profiles

It may be possible to represent the distribution of the velocity components u and w through the boundary layer by fewer than five parameters. The five quantities Θ_x , δ_x^* , Θ_z , δ_z^* and Θ_{xz} , could then be replaced by a smaller number of variables.

Mager (Reference 1) suggests the velocity profiles:

$$\frac{u}{U} = \left(\frac{y}{\delta} \right)^{\frac{1}{n}} \quad (9)$$

$$\frac{1}{\epsilon} \frac{w}{U} = \left(\frac{y}{\delta} \right)^{\frac{1}{n}} \left(1 - \frac{y}{\delta} \right)^m \quad (10)$$

where

$$\epsilon = \frac{\tau_{0z}}{\tau_{0x}} = \lim_{y \rightarrow 0} \frac{\frac{\partial w}{\partial y}}{\frac{\partial u}{\partial y}} \quad (11)$$

The use of ϵ introduces no new variables since it is the ratio of two quantities which also appear in the momentum integral equations.

ϵ seems to be a convenient "scale factor" between the cross flow and the main flow, for $\frac{1}{\epsilon} \frac{w}{U}$ and $\frac{u}{U}$ are of the same magnitude through a

good part of the boundary layer. If m and n are considered constants, the quantities defined in (4) through (8) are related by:

$$H \equiv \frac{\delta_x^*}{\theta_x} = \text{CONSTANT} \quad (12)$$

$$J \equiv \frac{1}{\epsilon} \frac{\theta_{xz}}{\theta_x} = \text{CONSTANT} \quad (13)$$

$$K \equiv \frac{1}{\epsilon} \frac{\delta_z^*}{\theta_x} = \text{CONSTANT} \quad (14)$$

$$L \equiv \frac{1}{\epsilon^2} \frac{\theta_z}{\theta_x} = \text{CONSTANT} \quad (15)$$

and Equations (2) and (3) can be expressed in terms of θ_x , ϵ and τ_{ox} . Mager found that values of $n = 7$, $m = 2$ gave velocity profiles which fitted the data of Reference 4, but not the data from Reference 7.

To determine the accuracy of assumptions concerning the u and w velocity profiles, we will compare assumed profiles to measured profiles from four sources:

1. Reference 4, Point 15, III
Flow through a 90° bend
2. Reference 7, Position 1a
Flow over a yawed wing
3. Reference 7, Position 1c
Flow over a yawed wing
4. Reference 6, Figure 9, $y/s = 0.5$
Wall boundary layer at the exit of a cascade of compressor blades

The profiles given by (9) and (10) with $n = 7$ and $m = 2$ are plotted in Figures 18 through 21 (dashed lines) along with data from the sources. The assumption of $n = 7$, $m = 2$ is only accurate for Figure 18 and different values of m and n must be used to describe the other data with any accuracy. The profiles given by (9) and (10), using values of m and n , which ~~cause integral quantities, (4) through (8) calculated from the assumed profiles to match the data,~~ are also shown in Figures 18, 19, 20

How matched

The value of H from the data,

m was chosen so that the values of H resulting from integrals matched 17.

and 21 (solid lines) along with the values of m and n used. The agreement is fair, but m and n must be considered variables in which case the momentum integral equations, (2) and (3), contain the variables θ_x , m and n , E & Re_x .

The use of δ to non-dimensionalize y , the distance from the wall, can make comparisons between assumed profiles and measured profiles uncertain, for δ is sometimes difficult to determine experimentally. In two-dimensional boundary-layer theory ($w = 0$), the momentum thickness*, θ , which can be accurately determined, is often used to normalize y ; when cross flows exist, θ_x can be used. For the two-dimensional turbulent boundary layer, Von Doenhoff and Tetervin (Reference 3) suggest a family of curves of $\frac{u}{U}$ vs. $\frac{y}{\theta}$ based on the parameter H , where

$$H = \frac{\delta^*}{\theta} \quad (16)$$

For a turbulent boundary layer with cross flow, the analogous parameter is

$$H = \frac{\delta_x^*}{\theta_x}$$

which will describe $\frac{u}{U}$ vs. $\frac{y}{\theta_x}$. Thus, a relationship

$$\frac{u}{U} = f\left(\frac{y}{\theta_x}, H\right) \quad (17)$$

can be established from the Von Doenhoff and Tetervin profiles.

An expression for the cross flow in terms of $\frac{y}{\theta_x}$, which retains the form of Equation (10) is

$$\frac{1}{\epsilon} \frac{w}{U} = \frac{u}{U} \left(1 - \frac{y}{a\theta_x}\right)^r \quad (18)$$

where $a = 10$.

The profiles given by Equations (17) and (18) as applied to data in References 4, 6 and 7 are plotted in Figures 22, 23, 24 and 25 along with the values of H and r used. ~~The values of H and r were again chosen so that the integral quantities (4) through (8) for the assumed profiles matched the measured values.~~ The Von Doenhoff and Tetervin profiles

*

$$\theta = \frac{1}{U^2} \int_0^d (U-u)u \, dy$$

} how matched

of $\frac{u}{U}$ vs. $\frac{y}{\theta_x}$ fit the data from the four sources with rather good accuracy, while the agreement in the cross flow profiles is fair.

The profiles based on H and r are compared to measurements made at points E, G, H, I and J_2 in the cascade, Section 3.2, in Figures 29 through 33. The agreement is only fair but it should be remembered that the accuracy of the measured data is poor. The quantity ϵ is particularly difficult to determine since the accuracy of angle measurement which depends on the dynamic head is very poor adjacent to the wall. The agreement between the assumed profiles and those measured is better in H, I and J_2 than in E and G. The cross flow at E and G is still strongly influenced by the inlet conditions which might be considered "artificial." Further along in the flow between G and H the original cross flow has been decelerated to zero and a "natural" cross flow, caused by the pressure field and shaped by the shear stresses begins. This crude description of occurrences may account for the differing agreement between the assumed profiles (which were suggested by observations of the "natural" cross flows) and the data.

The use of H instead of n to describe $\frac{u}{U}$ profile, improves the accuracy of describing the data but complicates mathematical manipulation, for the analytical relationship between $\frac{u}{U}$, $\frac{y}{\theta_x}$ and H is not known. However, the variation of θ_{xz} , θ_z and δ_z^* with H and r can be calculated numerically, then approximated by analytical expressions. It is evident from the definitions (4) through (8) that

$$\frac{1}{\epsilon} \frac{\theta_{xz}}{\theta_x} = \int_0^a \frac{u}{U} \left(1 - \frac{u}{U}\right) \left(1 - \frac{y}{a\theta_x}\right)^r d\left(\frac{y}{\theta_x}\right) = g(H, r) \quad (19)$$

$$\frac{1}{\epsilon} \frac{\delta_z^*}{\theta_x} = \int_0^a \frac{u}{U} \left(1 - \frac{y}{a\theta_x}\right)^r d\left(\frac{y}{\theta_x}\right) = h(H, r) \quad (20)$$

$$\frac{1}{\epsilon^2} \frac{\theta_z}{\theta_x} = \int_0^a \left(\frac{u}{U}\right)^2 \left(1 - \frac{y}{a\theta_x}\right)^r d\left(\frac{y}{\theta_x}\right) = l(H, r) \quad (21)$$

where g , h and l denote functional relationships.

These relationships are plotted in Figures 26, 27 and 28 and it appears that g , h and \downarrow can be approximated by simple functions of H and r .

B.1.3 Shear Stress Law

In two-dimensional boundary layer calculations, a relationship between τ_0 and θ , based on empirical results, is often assumed. Von Doenhoff and Tetervin suggest the Squire and Young formula

$$\frac{2\theta}{\tau_0} = \left[5.89 \log_{10} (4.075 R_\theta) \right]^2 \quad (22)$$

where $R_\theta = \frac{\theta U}{\nu}$

Gruschwitz (Reference 4) shows that a similar friction law

$$\frac{\tau_0}{2\theta} = \frac{0.01255}{R_\theta^{1/4}} \quad (23)$$

is applicable to τ_0 in a turbulent boundary layer with cross flow in a 90° bend.

B.1.4 Possible Solutions

Combining Equations (2) and (3) with the shear stress law, (22) or (23) and relations (12), (19), (20) and (21) results in two partial differential equations in the four variables θ_x , H , ϵ and r . Two more equations relating the four quantities are required before any solution can be attempted. The simplest case, that of H and r (or m and n) being constant, has been treated by Mager (Reference 1). The profiles in Figure 18 were found representative of the boundary layer flow through a 90° bend and the relationships (12) through (15) were used with (23) to express the momentum integral equations in two dependent variables, θ_x and ϵ . For ϵ small compared to 1, a first approximation to the solution was obtained, while for ϵ appreciable compared to 1, a more complicated second approximation to the solution is presented. The agreement between calculations and measurements was fair.

If H and r are not constant, but their variations are known, solutions still might be possible. However, an a priori knowledge of H and r for a flow is unlikely so it seems that two more general relationships between θ_x , H , ϵ and r must be discovered.

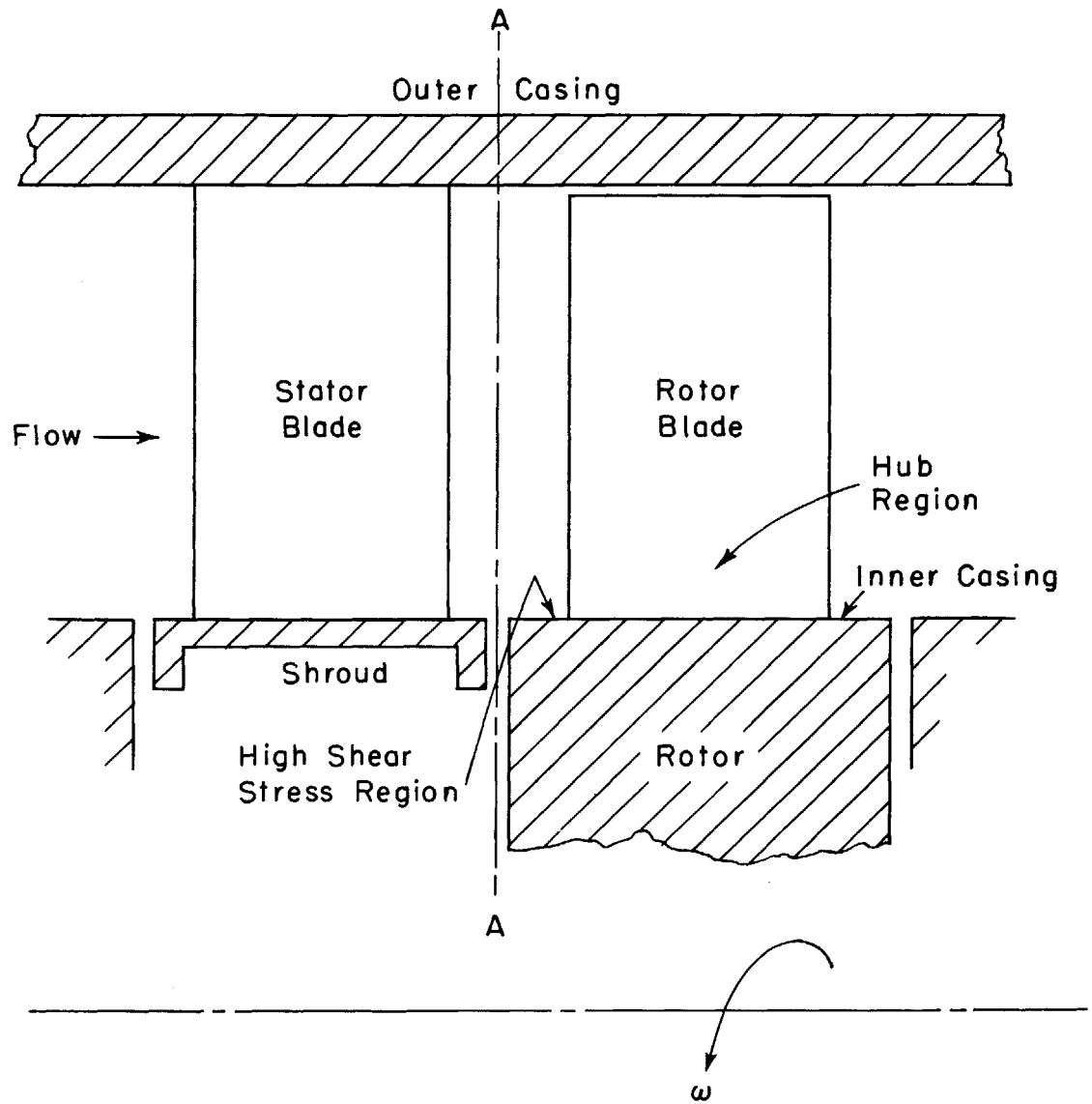
TABLE I

BOUNDARY-LAYER QUANTITIES*

Position	B	E	G	H	I	J ₂	A	C	D	F	J ₁	J ₃
θ_x^*	.0523	.0437	.0474	.0518	.0604	.0761	.0506	.0522	.0347	.0532	.159	.0426
δ_x^*	.0598	.0545	.0558	.0718	.0771	.1034	.0564	.0670	.0406	.0697	.253	.0596
θ_z	.0139	.0037	.00311	.00081	.00063	.00659	.0180	.00944	.00374	.00280	.00205	.00083
δ_z^*	-.0434	-.0308	-.0124	.0063	.0105	.0294	-.0682	-.0448	-.0362	-.0348	.0284	.0108
θ_{zx}	-.00702	-.00366	-.00122	.00168	.0029	.00941	-.0559	-.0376	-.0334	-.0292	.0168	.0086
H	1.14	1.25	1.18	1.39	1.28	1.36	1.11	1.28	1.17	1.31	1.59	1.40
β	53.5	51.5	45.0	36.5	31.5	22.5	62.0	52.0	60.0	51.0	25.0	29.0
ϵ_i	-.4142	-.1737	-.0436	.0959	.1478	.3007	-.3739	-.4452	-.1673	-.2217	.1763	.1495

* Defined by Mager (Reference 2).

Quantity in inches
 β in degrees



CONFIGURATION AT THE HUB OF A COMPRESSOR WITH SHROUDED STATOR ROOTS

FIGURE 1

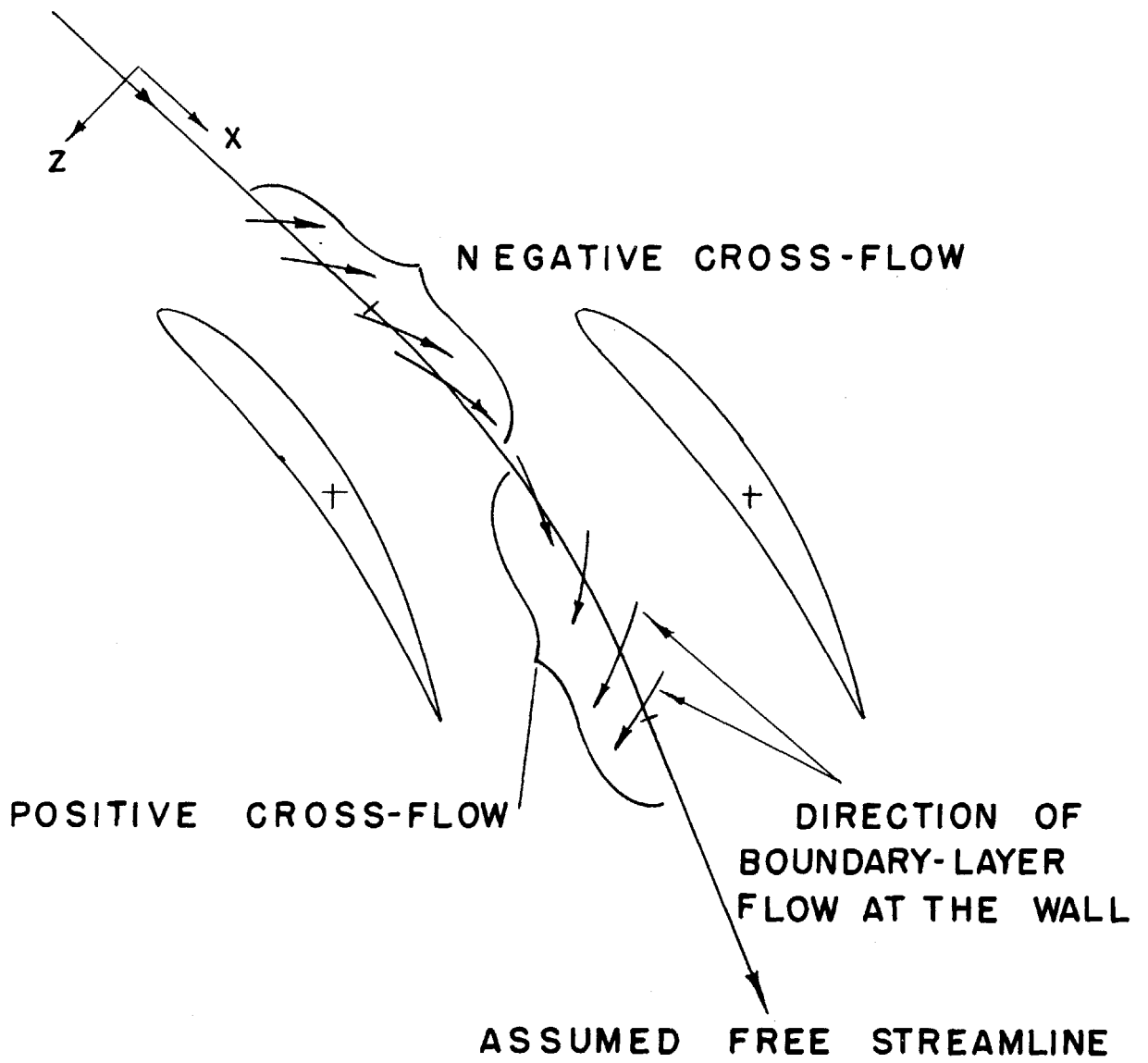
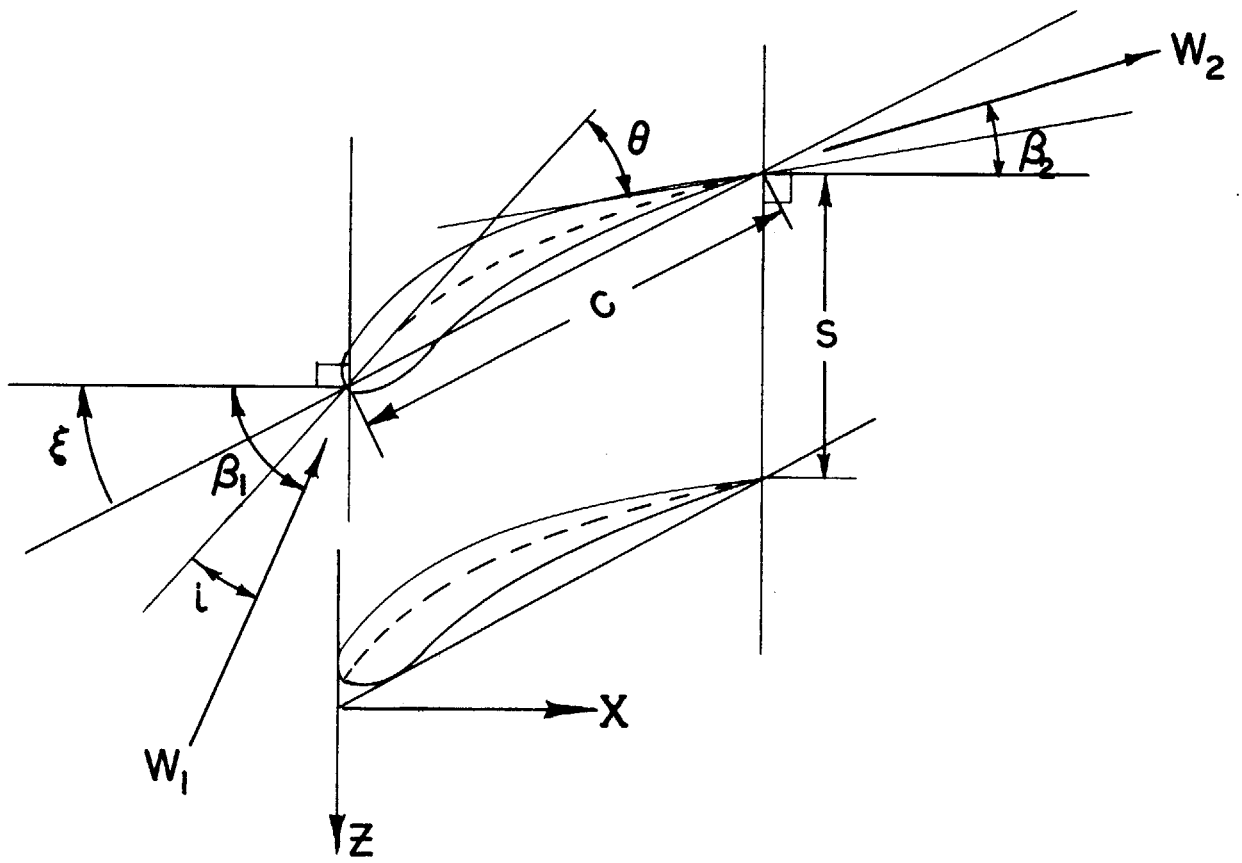


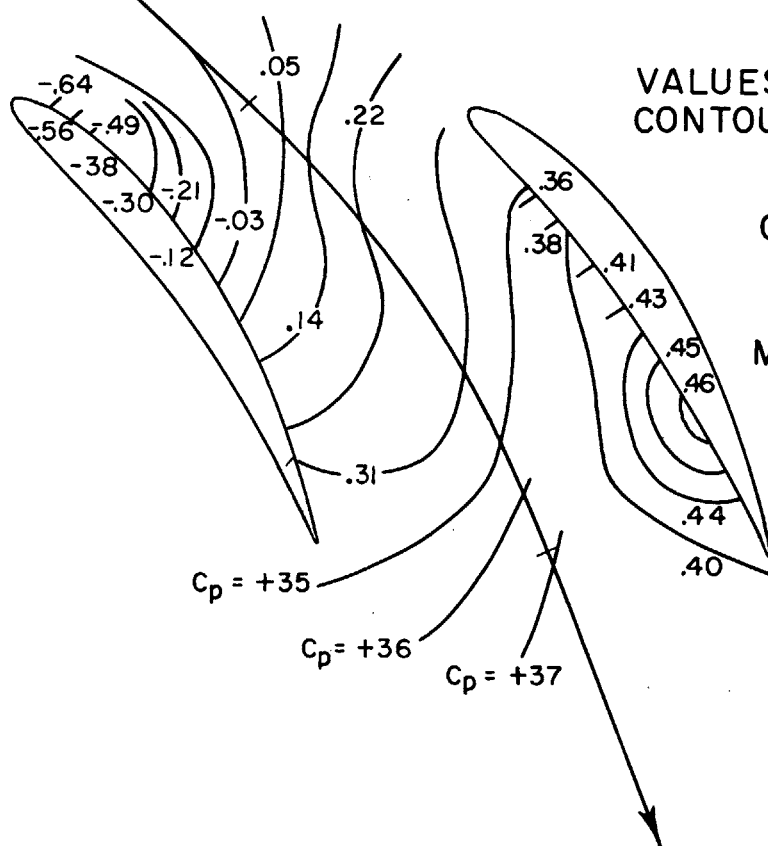
FIGURE 2



DEFINITION OF CASCADE GEOMETRY

FIGURE 3

① ASSUMED FREE STREAMLINE

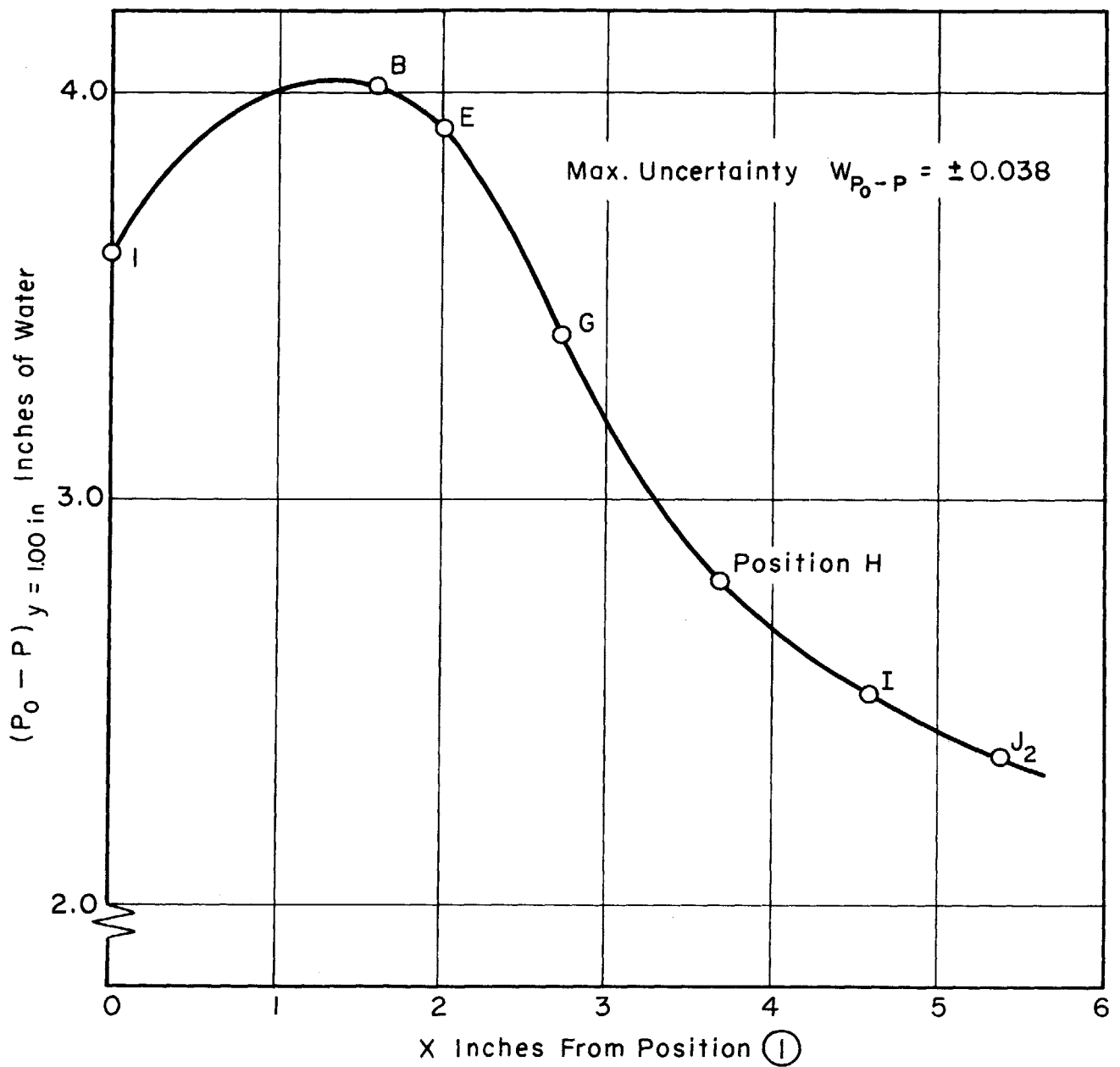


VALUES INDICATE
CONTOURS OF C_p

$$C_p = \frac{P - P_1}{(P_0 - P)_1}$$

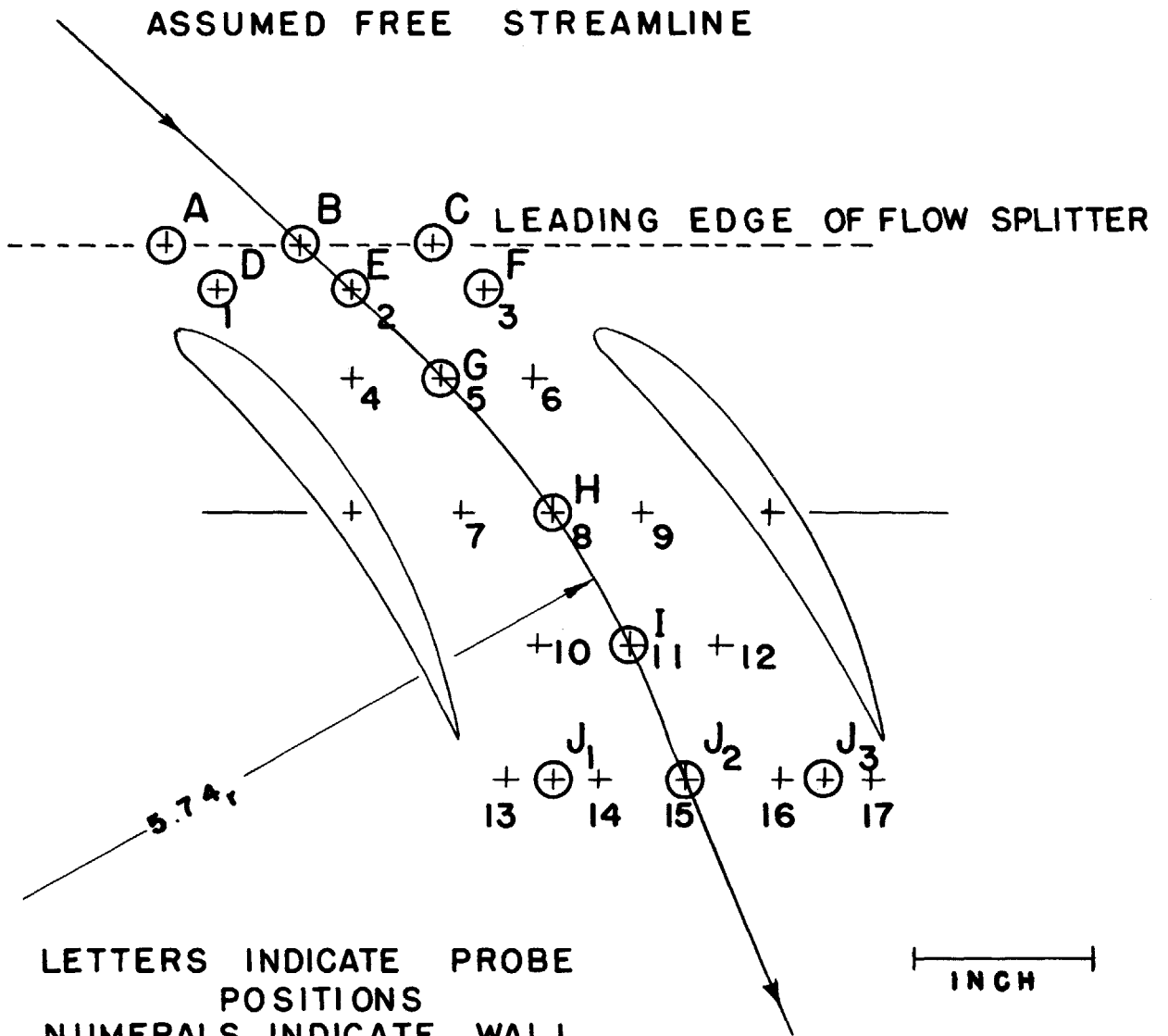
MAX. UNCERTAINTY
 $W_{C_p} = \pm 0.038$

WALL STATIC PRESSURE CONTOURS
FIGURE 4



DYNAMIC HEAD DISTRIBUTION ALONG ASSUMED FREE STREAM-LINE OUTSIDE OF BOUNDARY - LAYER

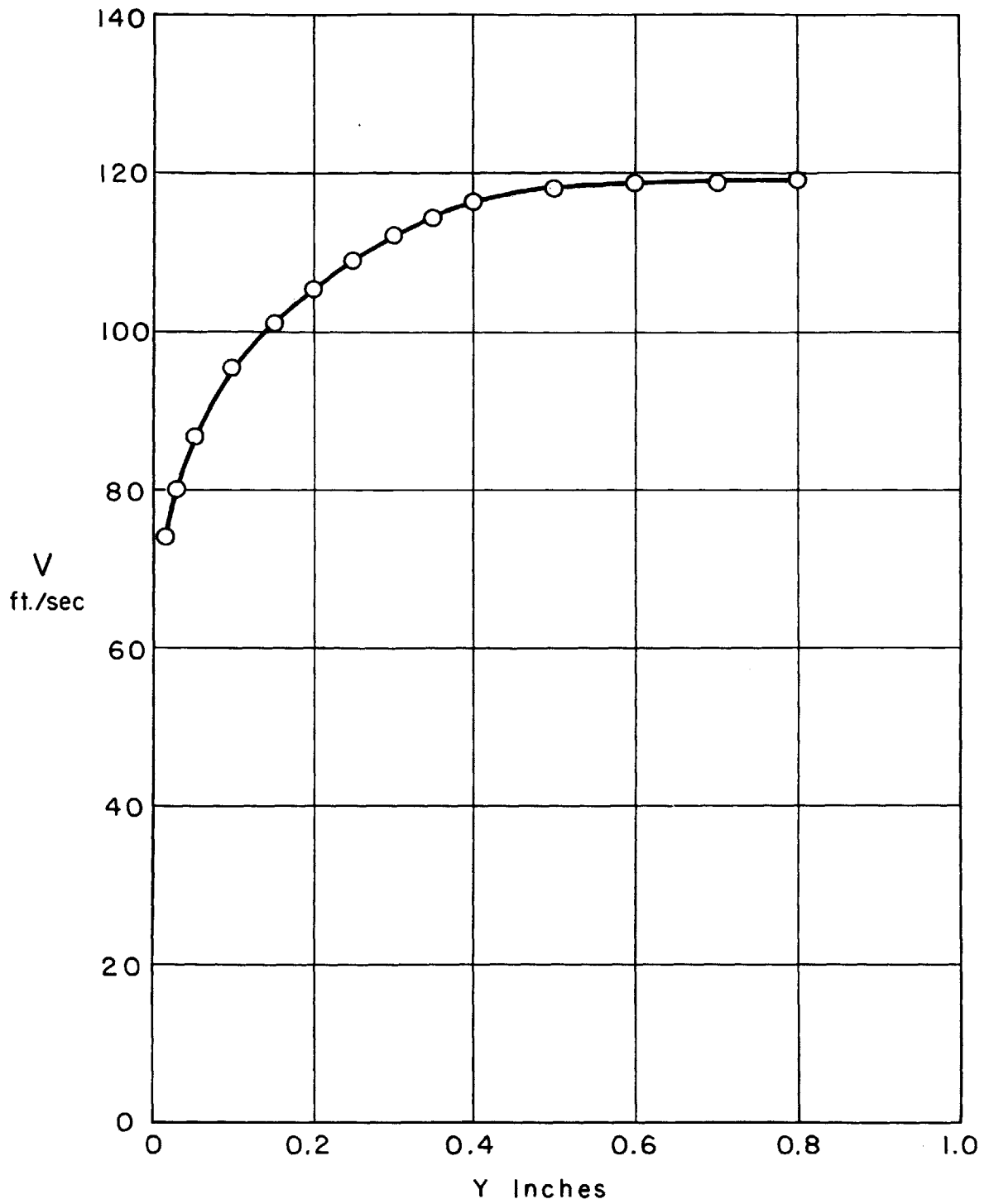
FIGURE 5



LETTERS INDICATE PROBE
 POSITIONS
 NUMERALS INDICATE WALL
 STATIC TAPS
 FIGURE IS FULL SIZE AND
 DIMENSIONS MAY BE SCALED

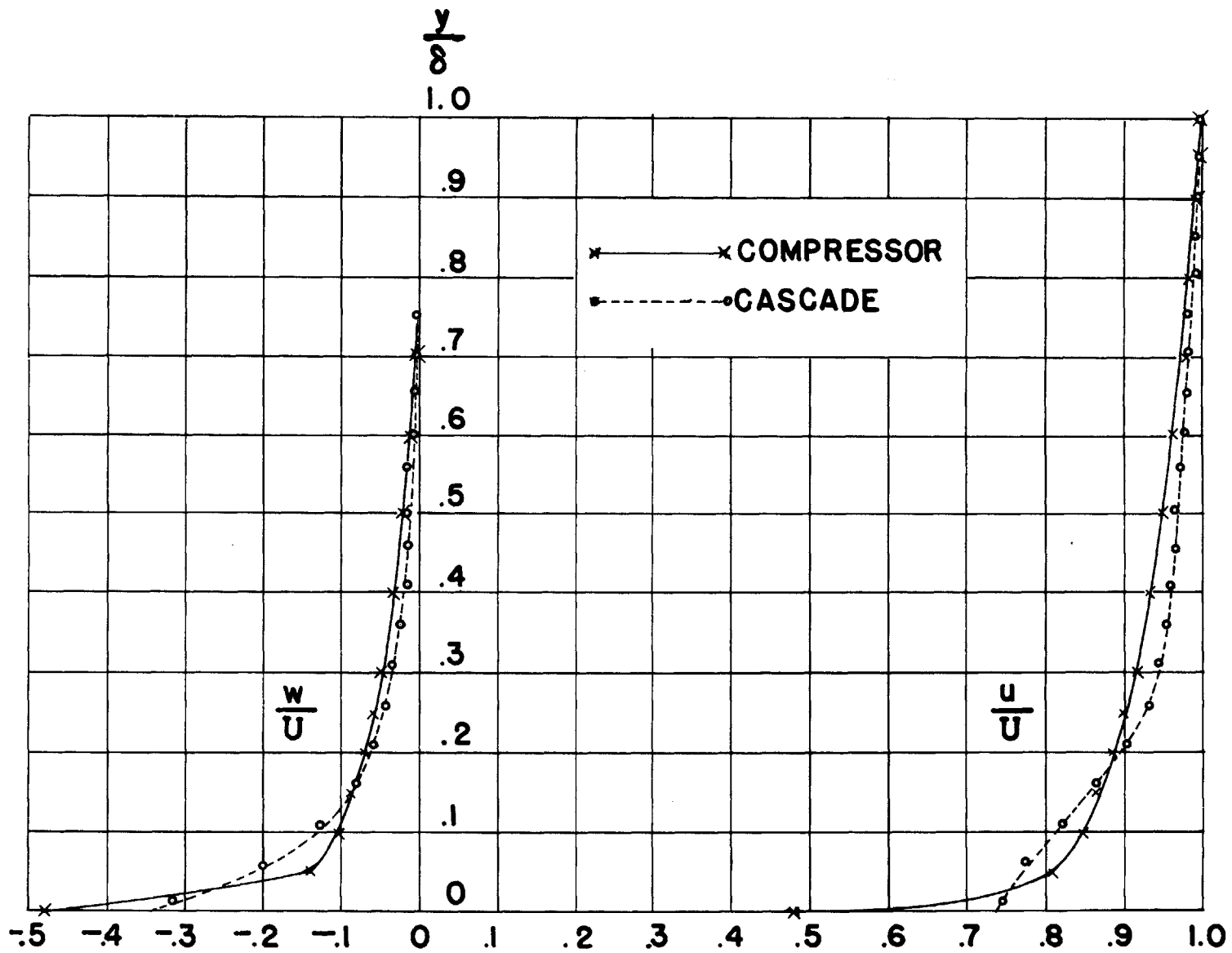
LOCATION OF PROBE POSITIONS AND
 STATIC WALL TAPS

FIGURE 6



DISTRIBUTION OF INLET VELOCITY RELATIVE TO
STATIONARY HUB

FIGURE 7



BOUNDARY-LAYER PROFILES FOUND IN COMPRESSOR AND
IN CASCADE AT POSITION B

FIGURE 8

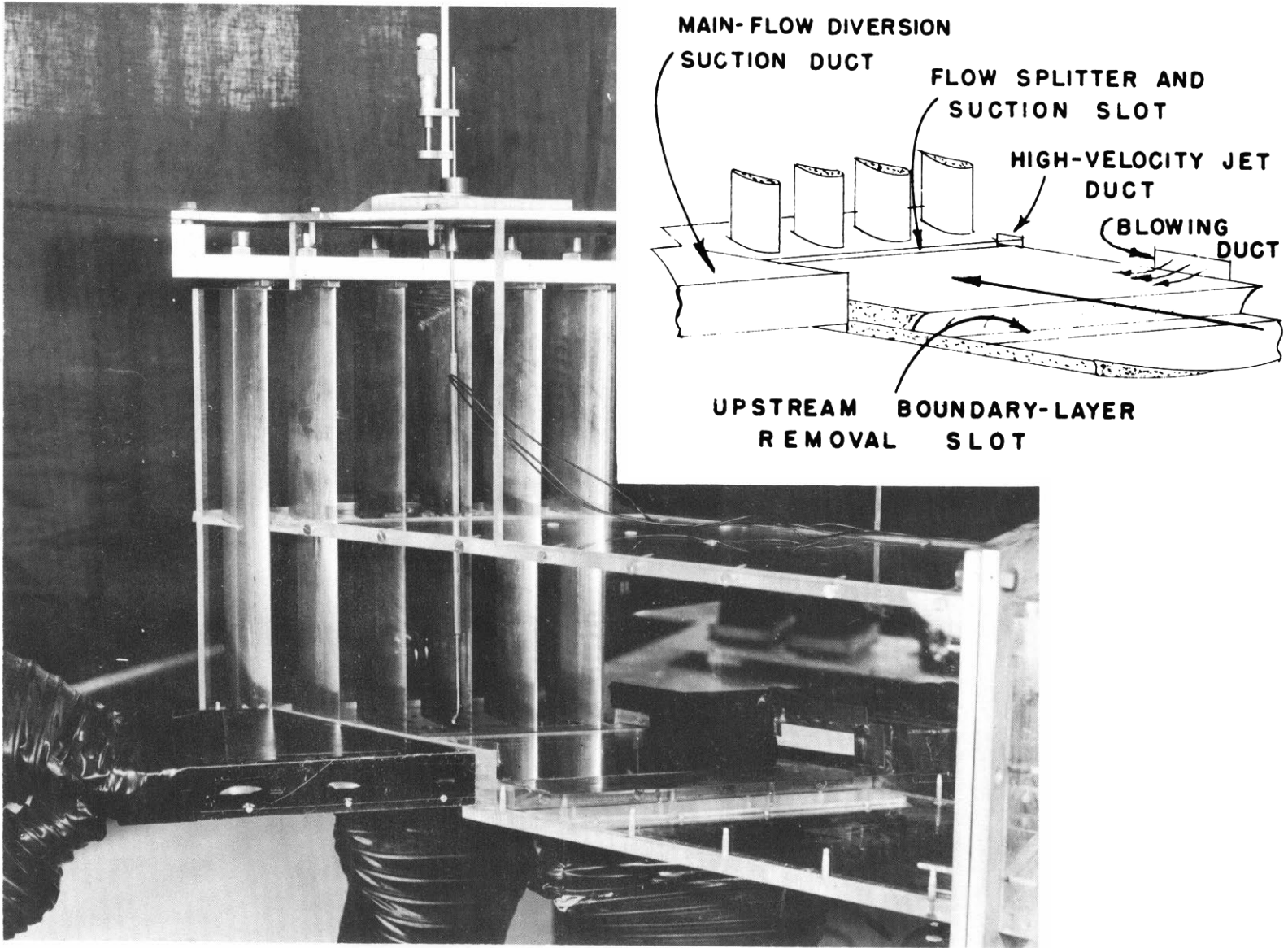
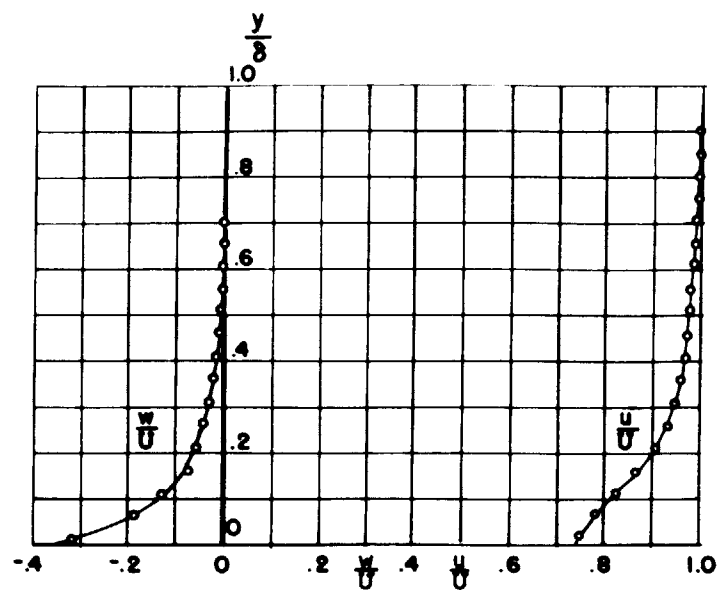


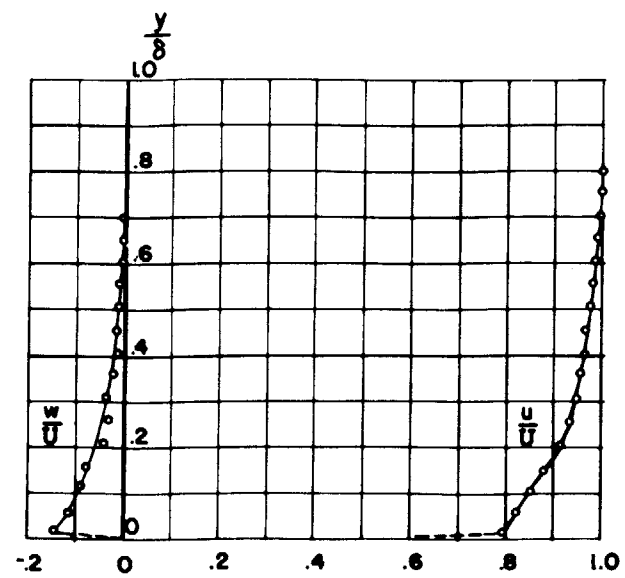
FIGURE 9

BOUNDARY-LAYER PROFILES ALONG ASSUMED FREE STREAMLINE

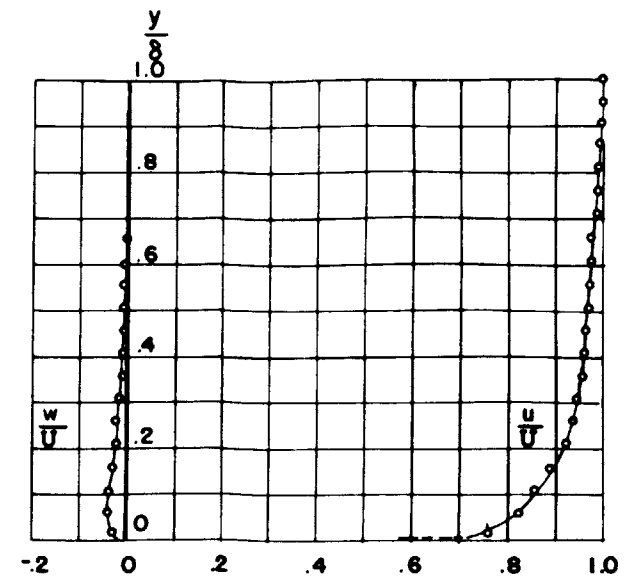
FIGURE 10



POSITION B
x=0



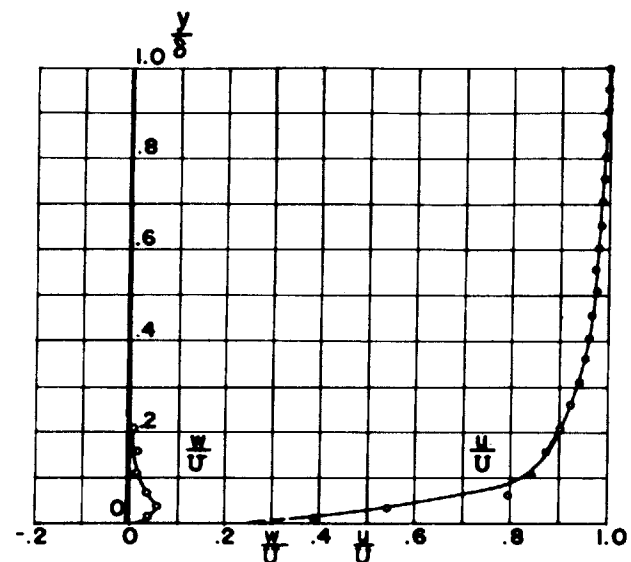
POSITION E
x=0.40 in



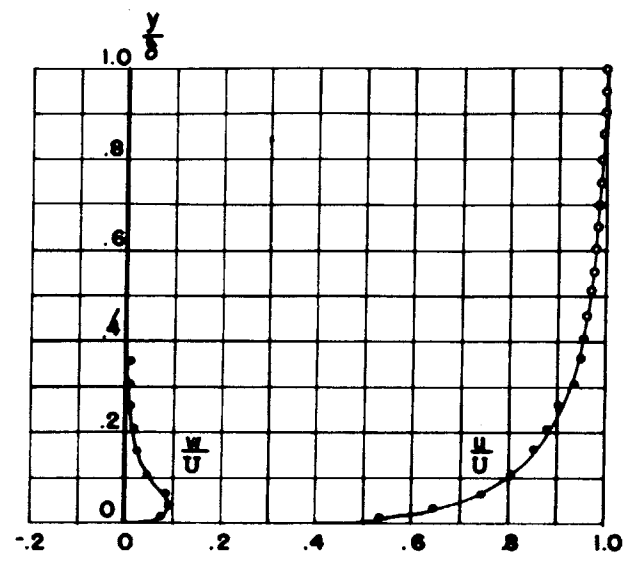
POSITION G
x=1.13 in

MAX. UNCERTAINTY : $w_{\frac{u}{U}} = \pm 0.018$
 $w_{\frac{w}{U}} = \pm 0.008$
 $w_{\frac{y}{\delta}} = \pm 0.002$

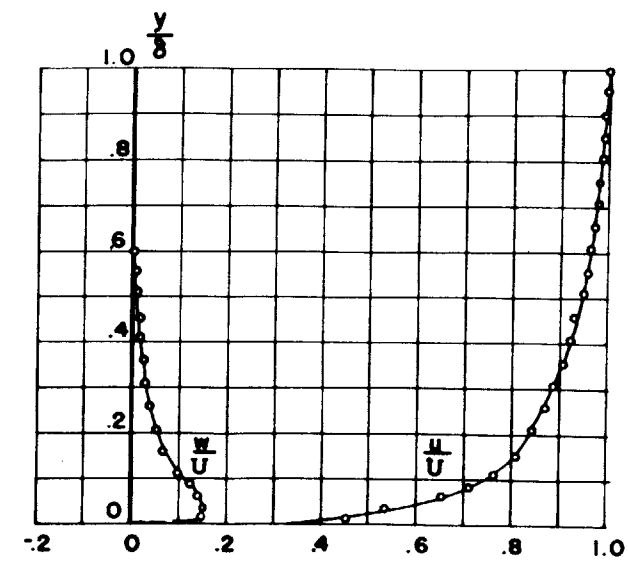
FOR ALL POSITIONS $\delta = 1.00$ in.



POSITION H
x=2.09 in



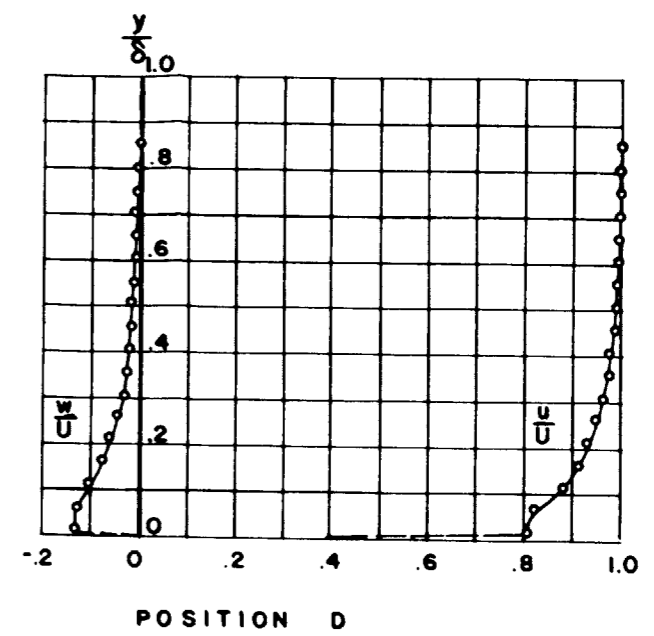
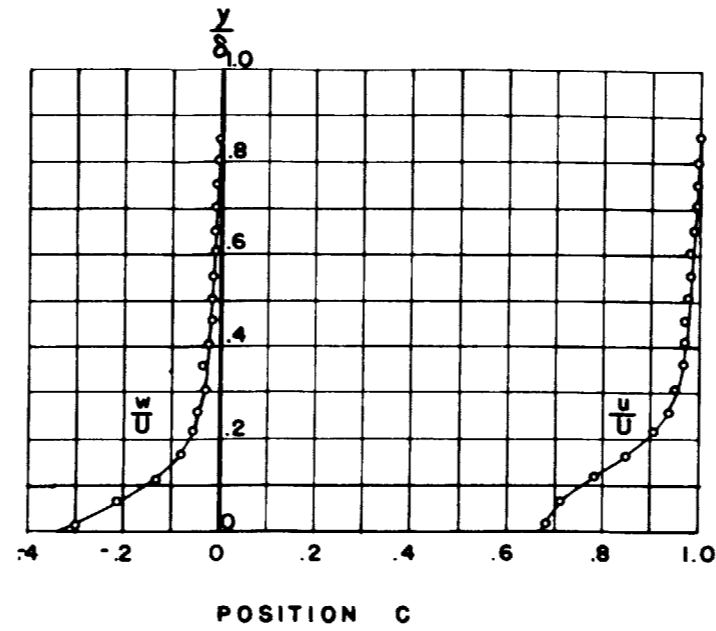
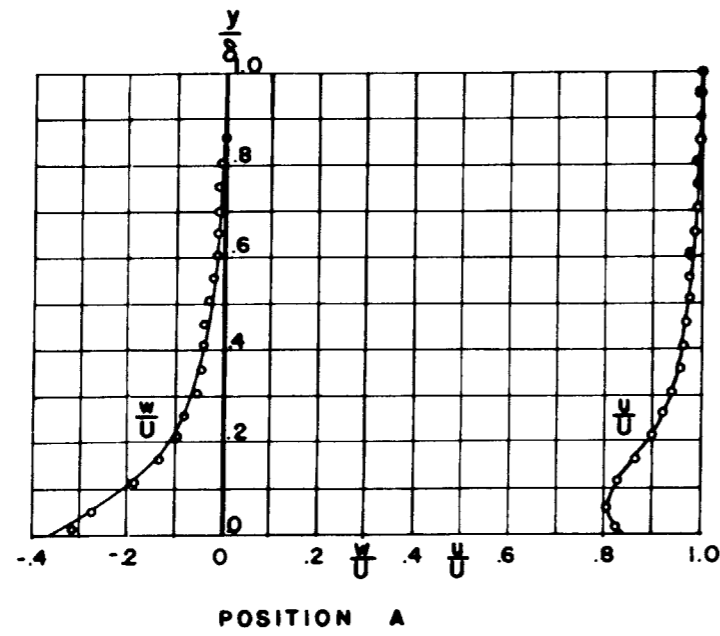
POSITION I
x=2.96 in



POSITION J₂
x=3.78 in

BOUNDARY-LAYER PROFILES

FIGURE II

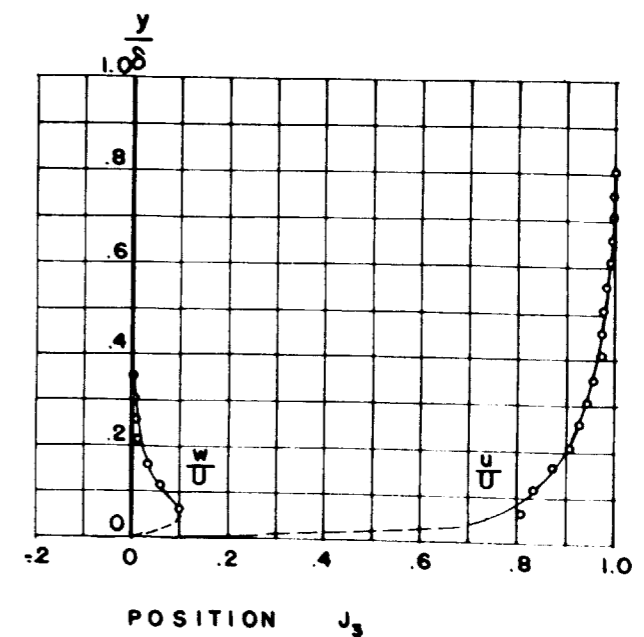
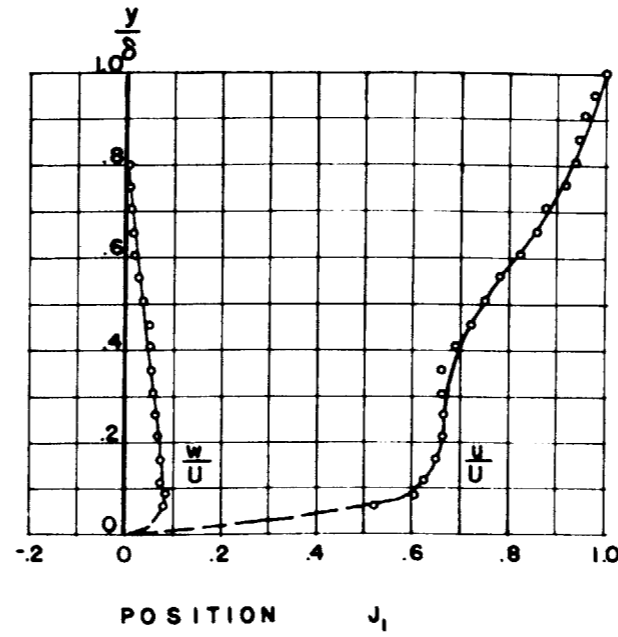
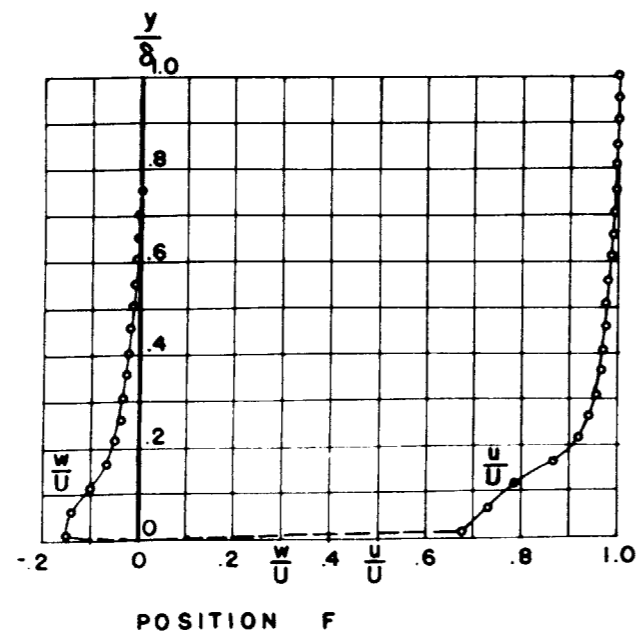


MAX. UNCERTAINTY : $w_{\frac{U}{U_{\infty}}} = \pm 0.018$

FOR ALL POSITIONS $\delta = 1.00$ in.

$w_{\frac{W}{U_{\infty}}} = \pm 0.008$

$w_{\frac{y}{\delta_0}} = \pm 0.002$

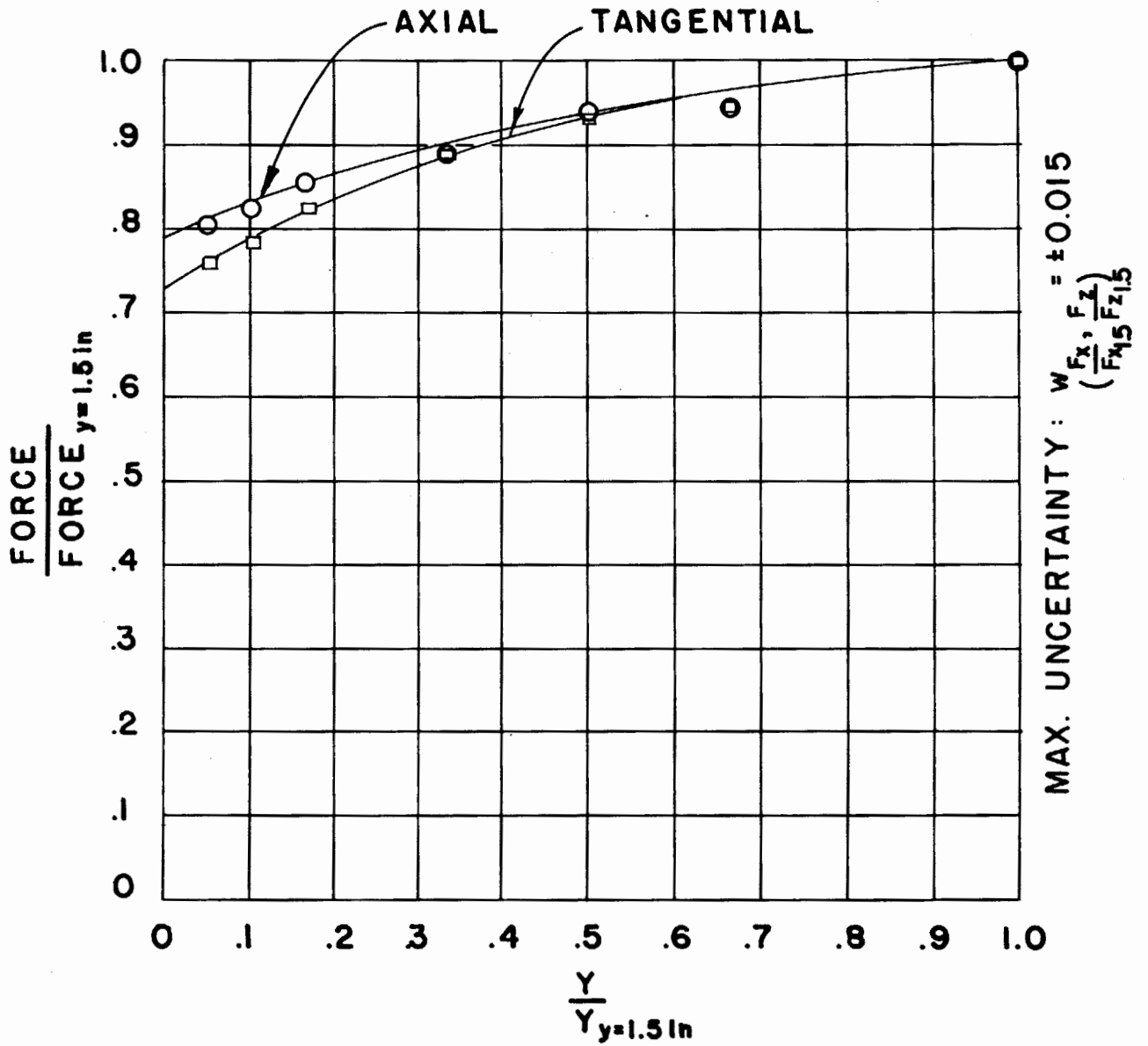


FLOW
→
DIRECTION



CARBON BLACK TRACES ON BOTTOM WALL OF
CASCADE WITH SKEWED INLET WALL BOUNDARY-LAYER

FIGURE 12



AXIAL AND TANGENTIAL FORCE DISTRIBUTION

FIGURE 13

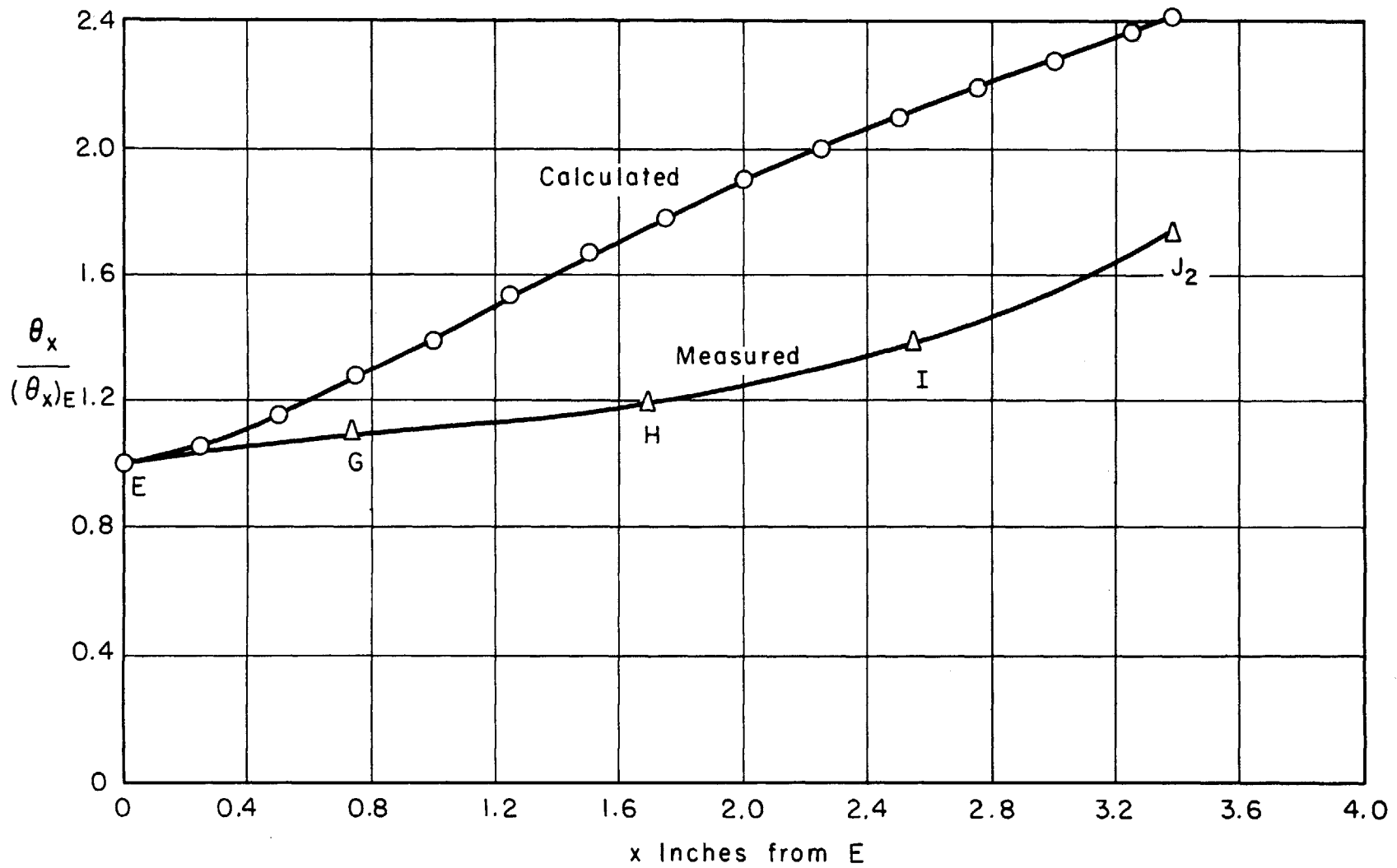


FIG. 14 - GROWTH OF θ_x ALONG CENTER STREAMLINE OF CASCADE IN REFERENCE 5, MEASURED AND CALCULATED (SECTION 3.3)

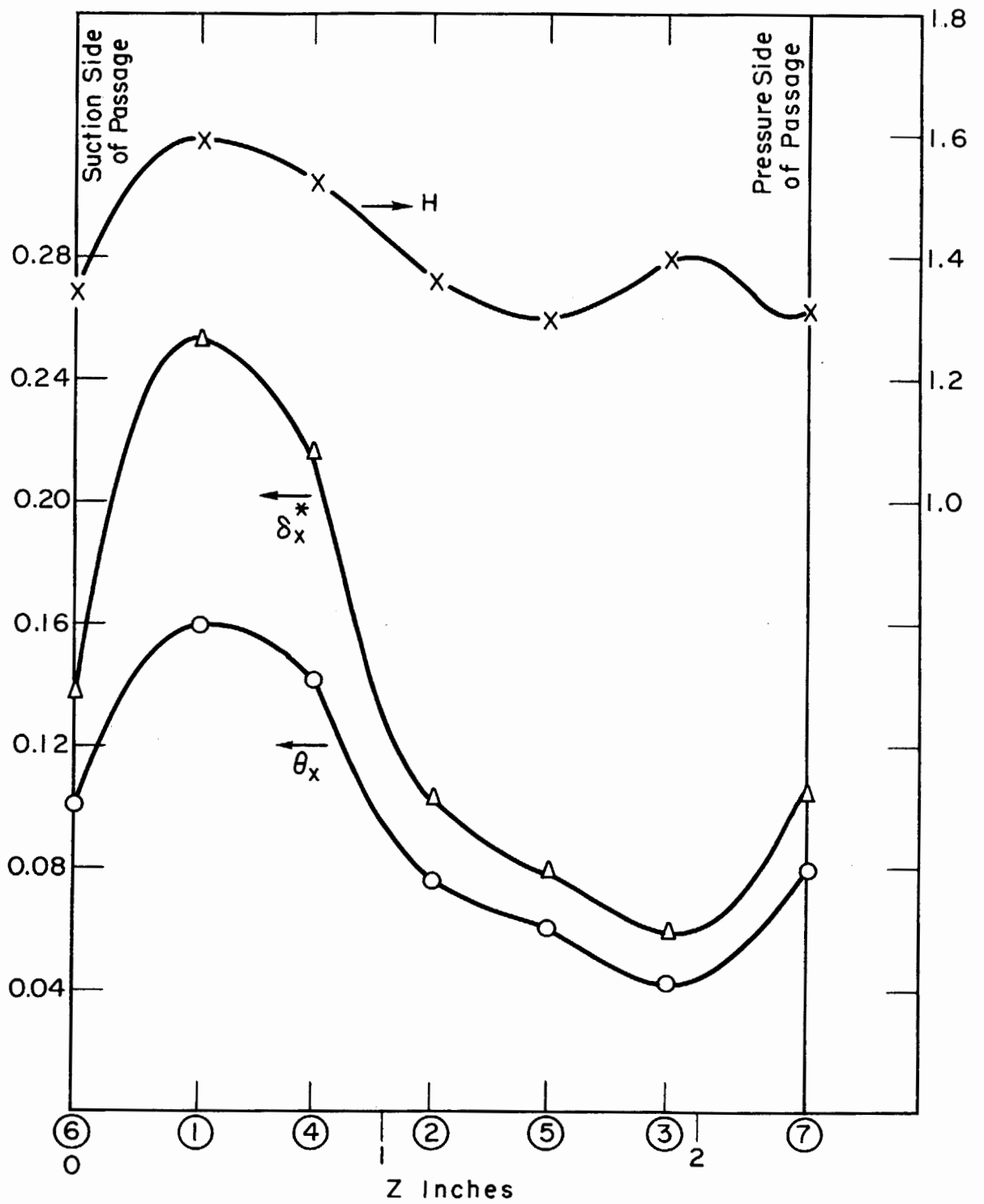


FIG. 15 - SHAPE PARAMETERS VS. TANGENTIAL POSITION Z AT AT EXIT PLANE OF CASCADE (REFERENCE 5)

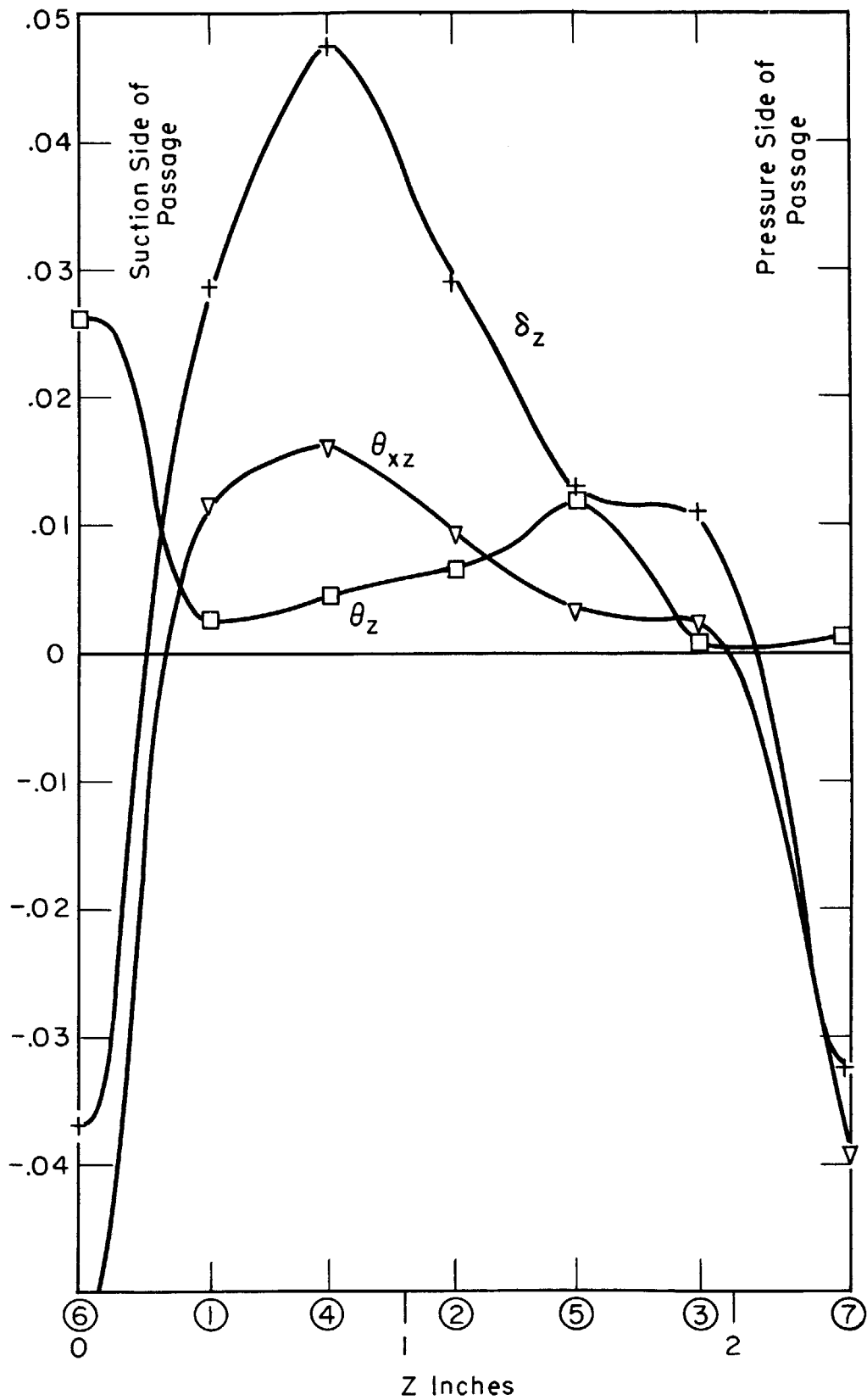
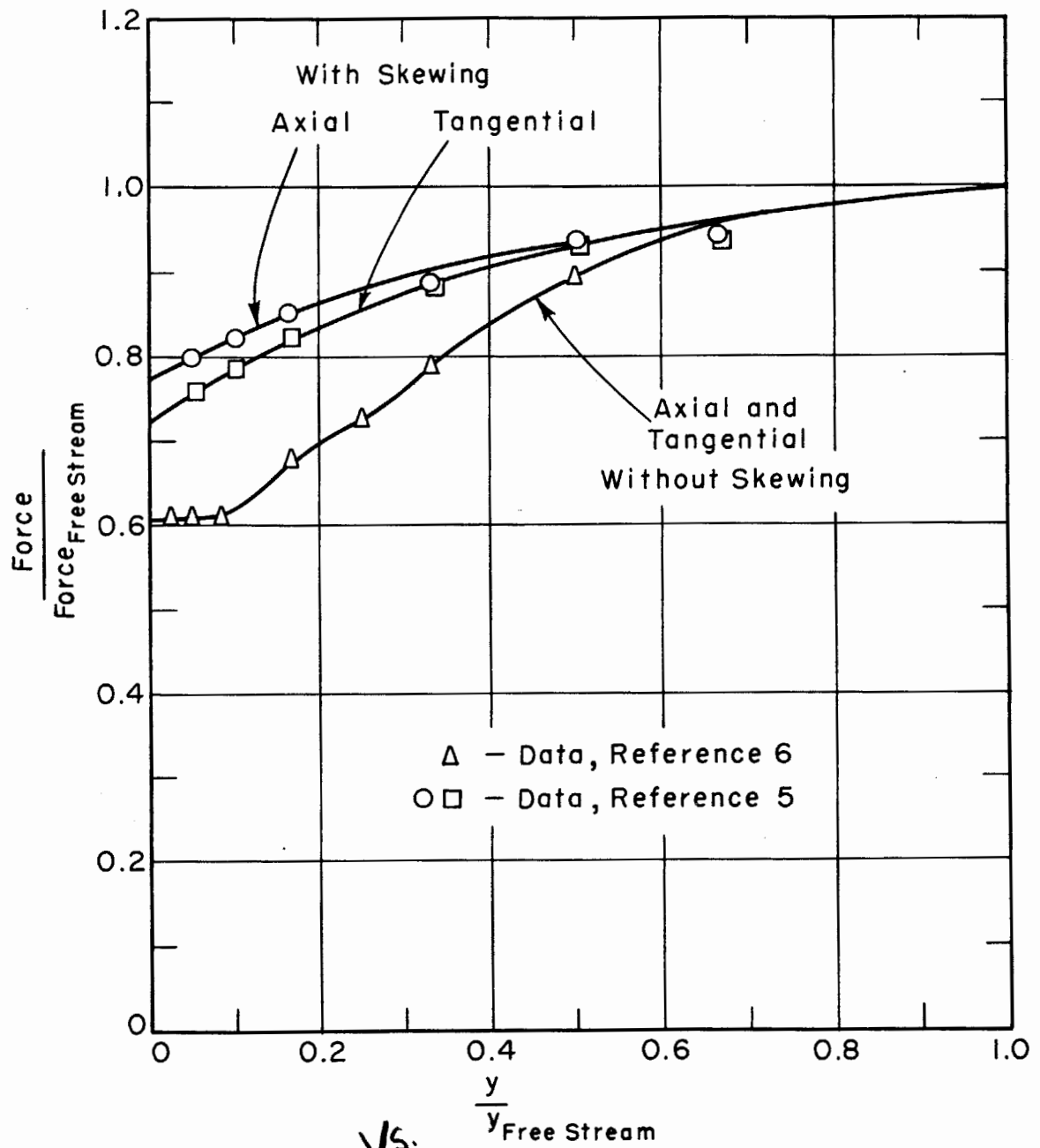


FIG. 16 - SHAPE PARAMETERS VS. TANGENTIAL POSITION Z AT EXIT PLANE OF CASCADE (REFERENCE 5).



BLADE FORCES ^{vs.} S. SPANWISE POSITION WITH AND WITHOUT BOUNDARY-LAYER SKEWING

FIGURE 17

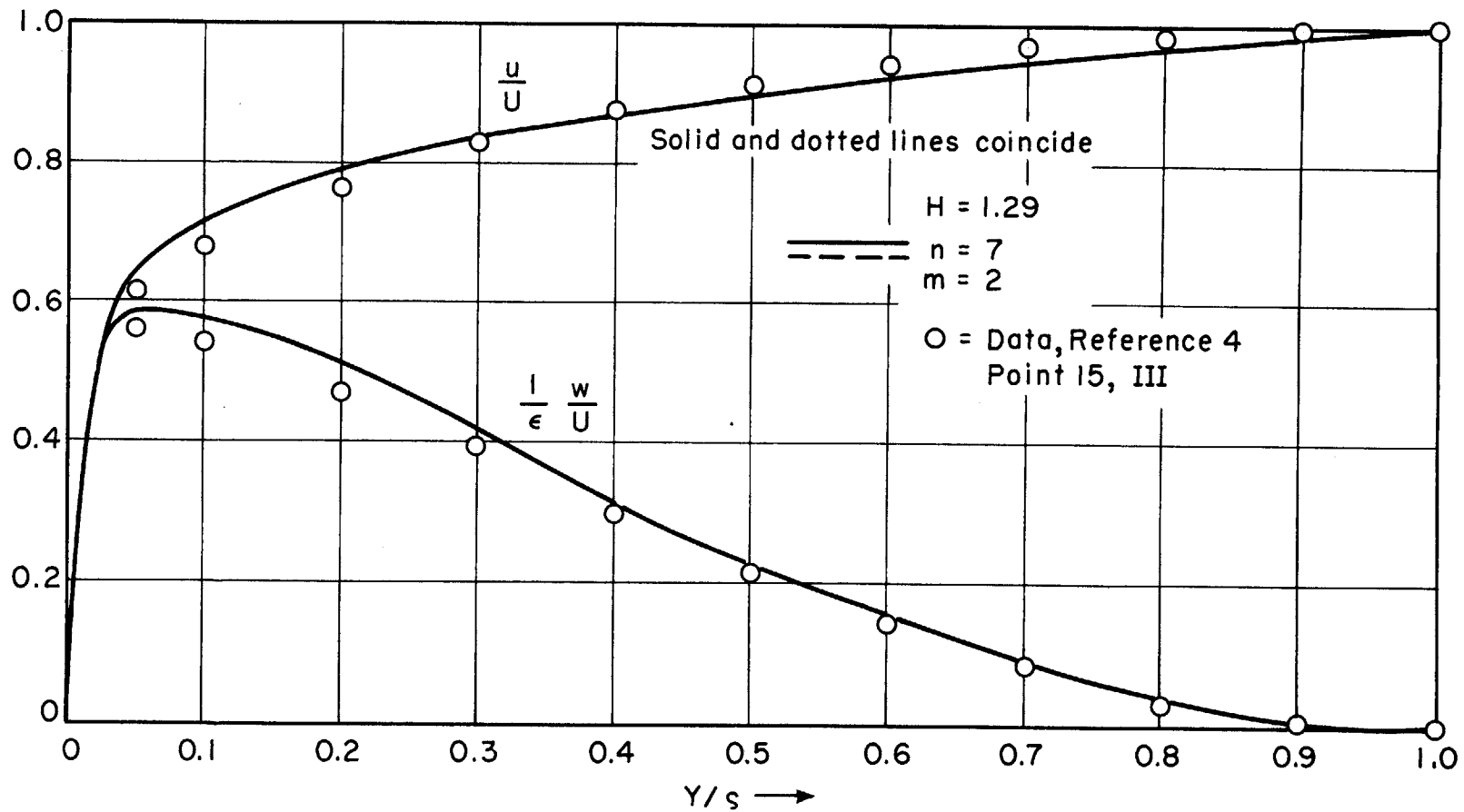


FIG. 18 - COMPARISON OF VELOCITY PROFILES ON THE BASIS OF m AND n WITH EXPERIMENTAL DATA FROM REFERENCE 4 POINT 15, III

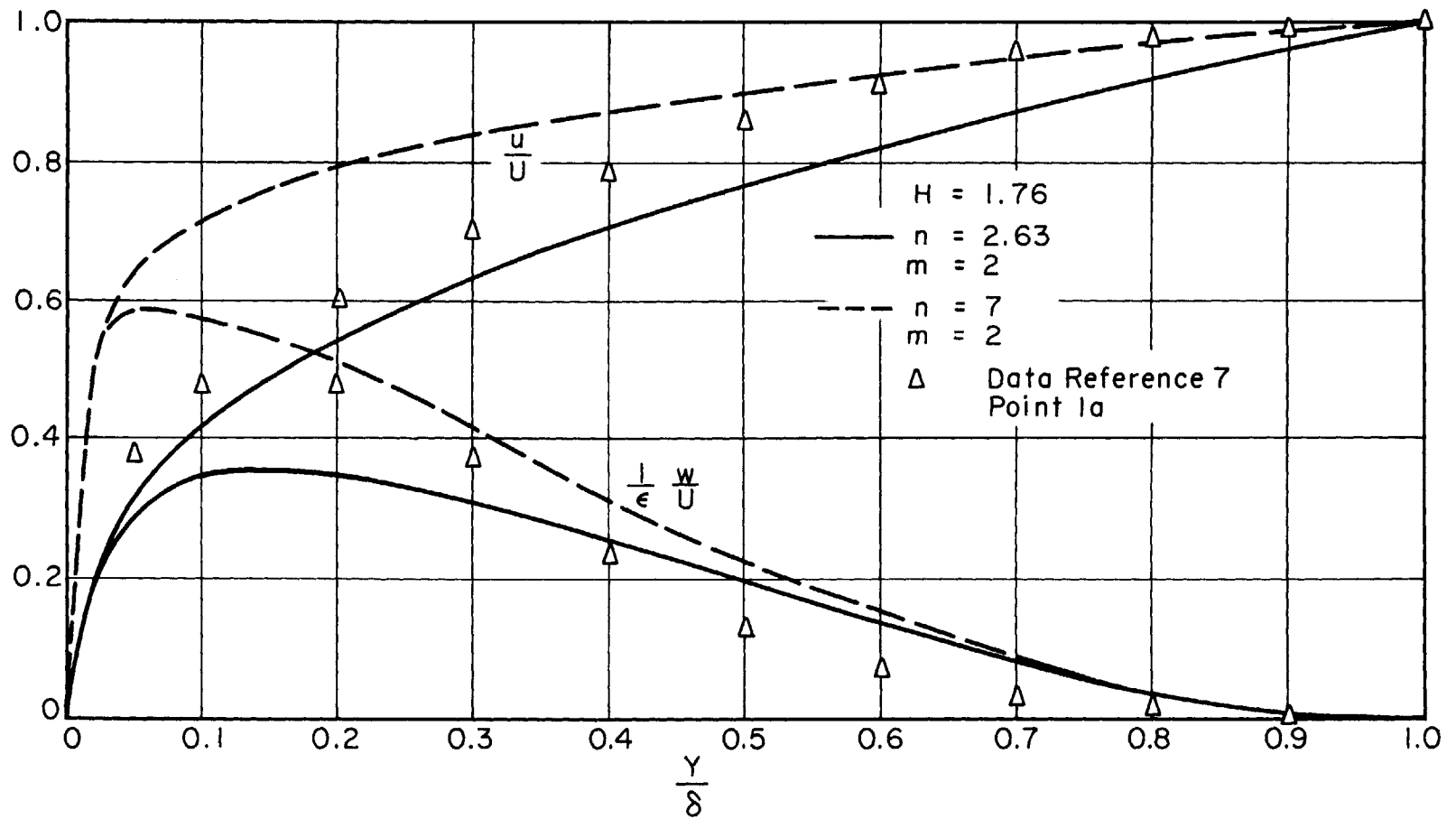


FIG. 19 - COMPARISON OF VELOCITY PROFILES ON THE BASIS OF m AND n WITH EXPERIMENTAL DATA FROM REFERENCE 7, POSITION 1a

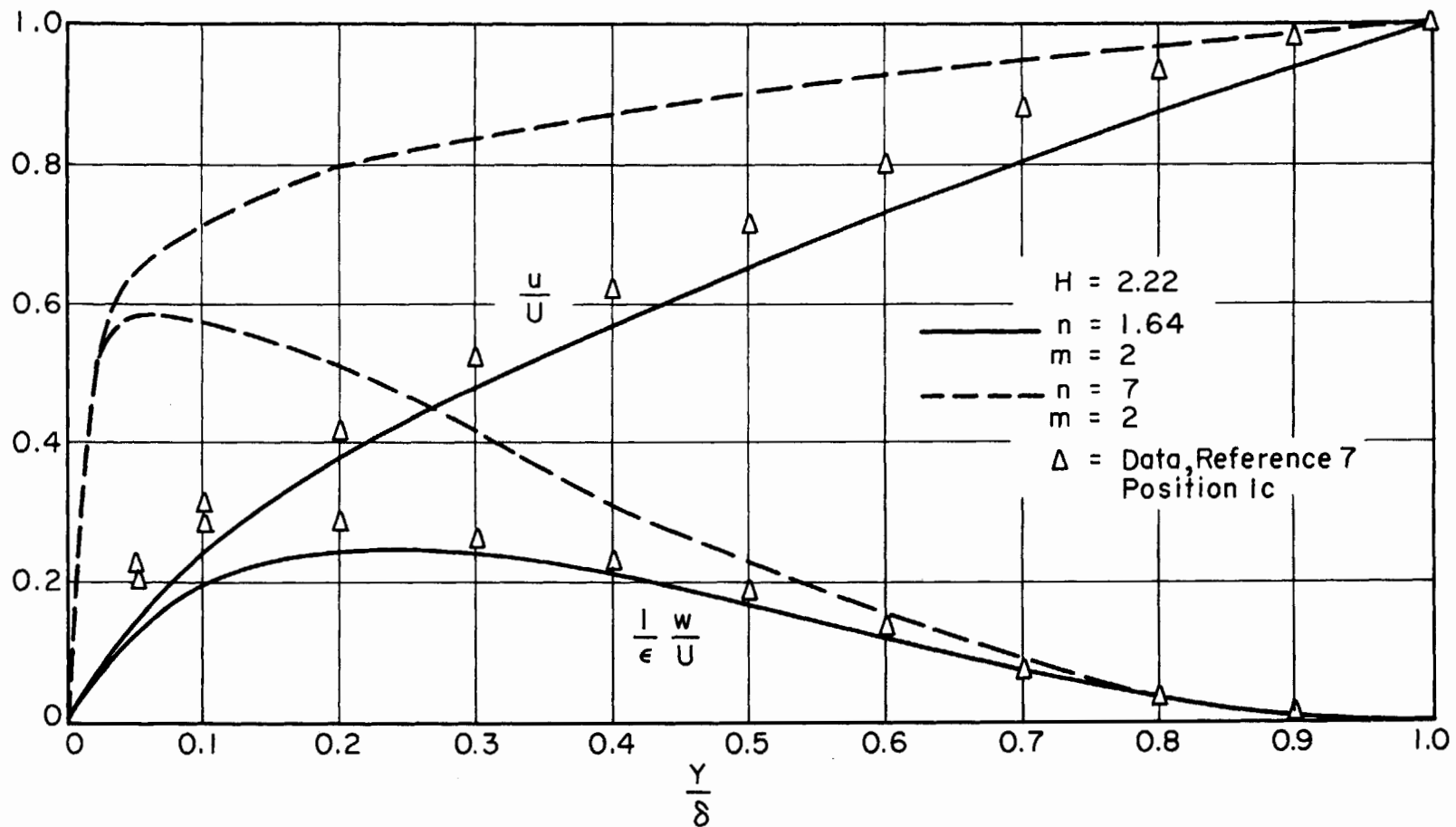


FIG. 20 - COMPARISON OF VELOCITY PROFILES ON THE BASIS OF m AND n WITH EXPERIMENTAL DATA FROM REFERENCE 7 POSITION 1c

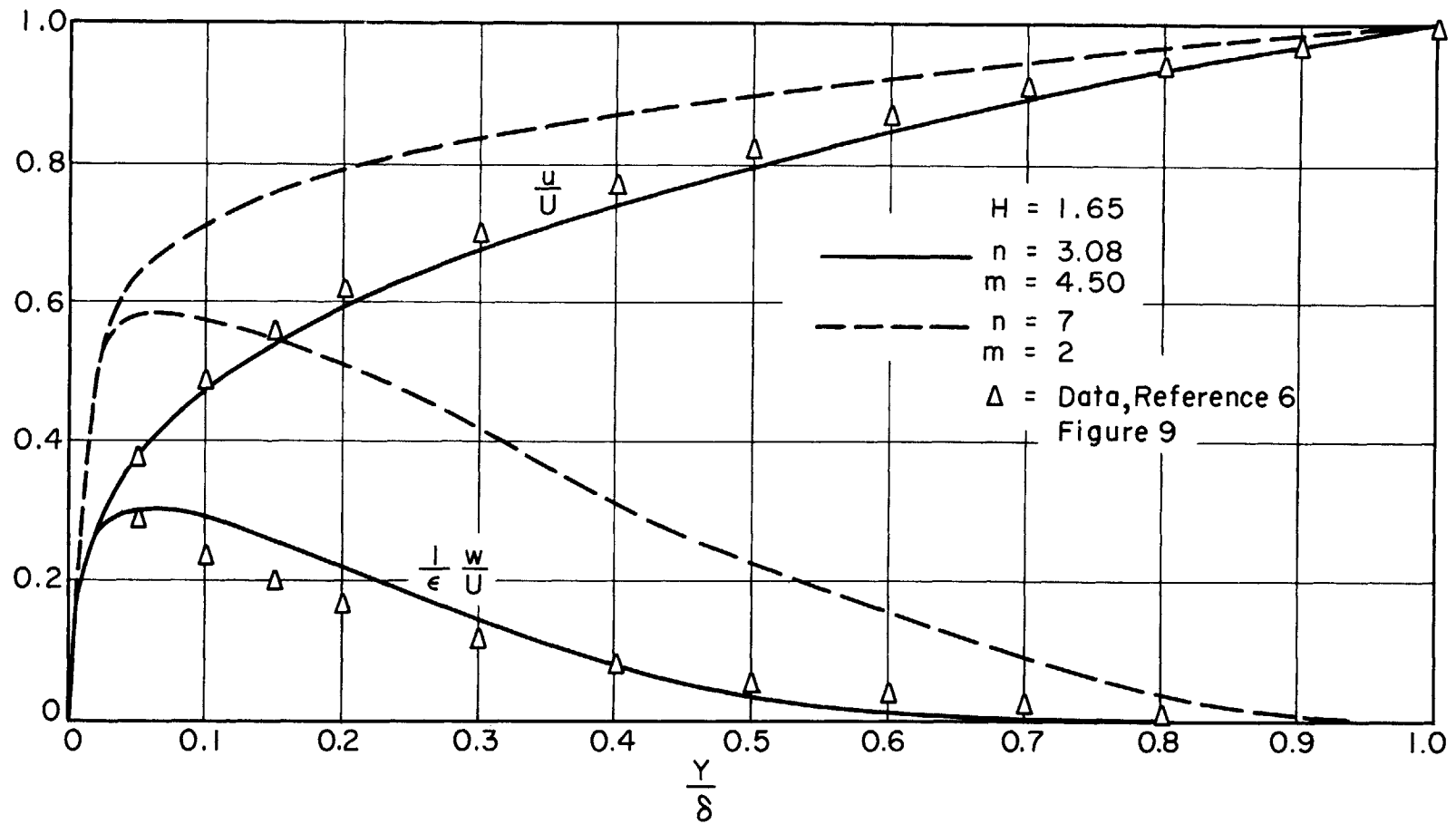


FIG. 21 - COMPARISON OF VELOCITY PROFILES ON THE BASIS OF m AND n WITH EXPERIMENTAL DATA FROM REFERENCE 6 FIGURE 9

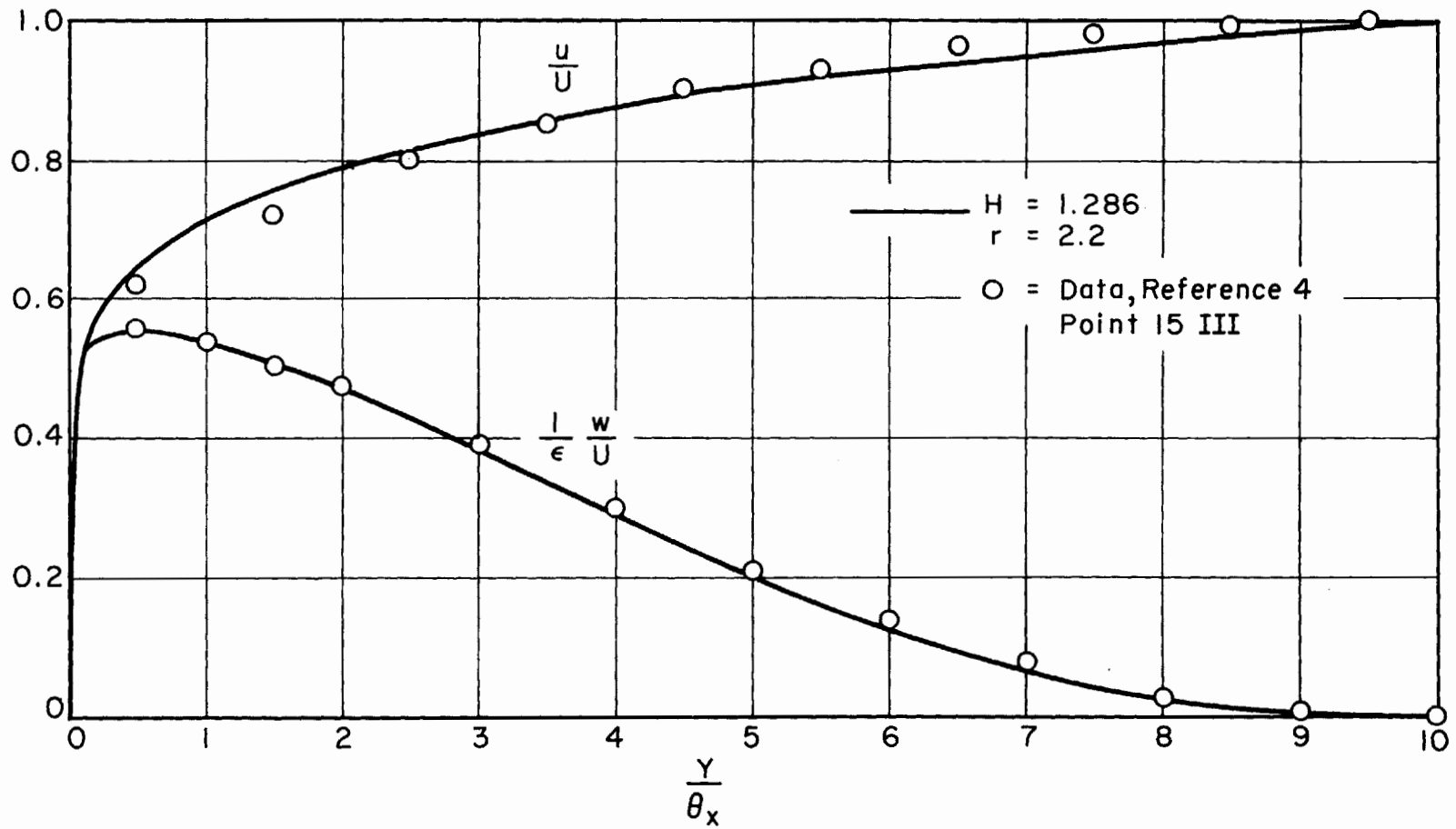


FIG. 22 - COMPARISON OF VELOCITY PROFILES ON THE BASIS OF H AND r WITH EXPERIMENTAL DATA FROM REFERENCE 4 POINT 15 III

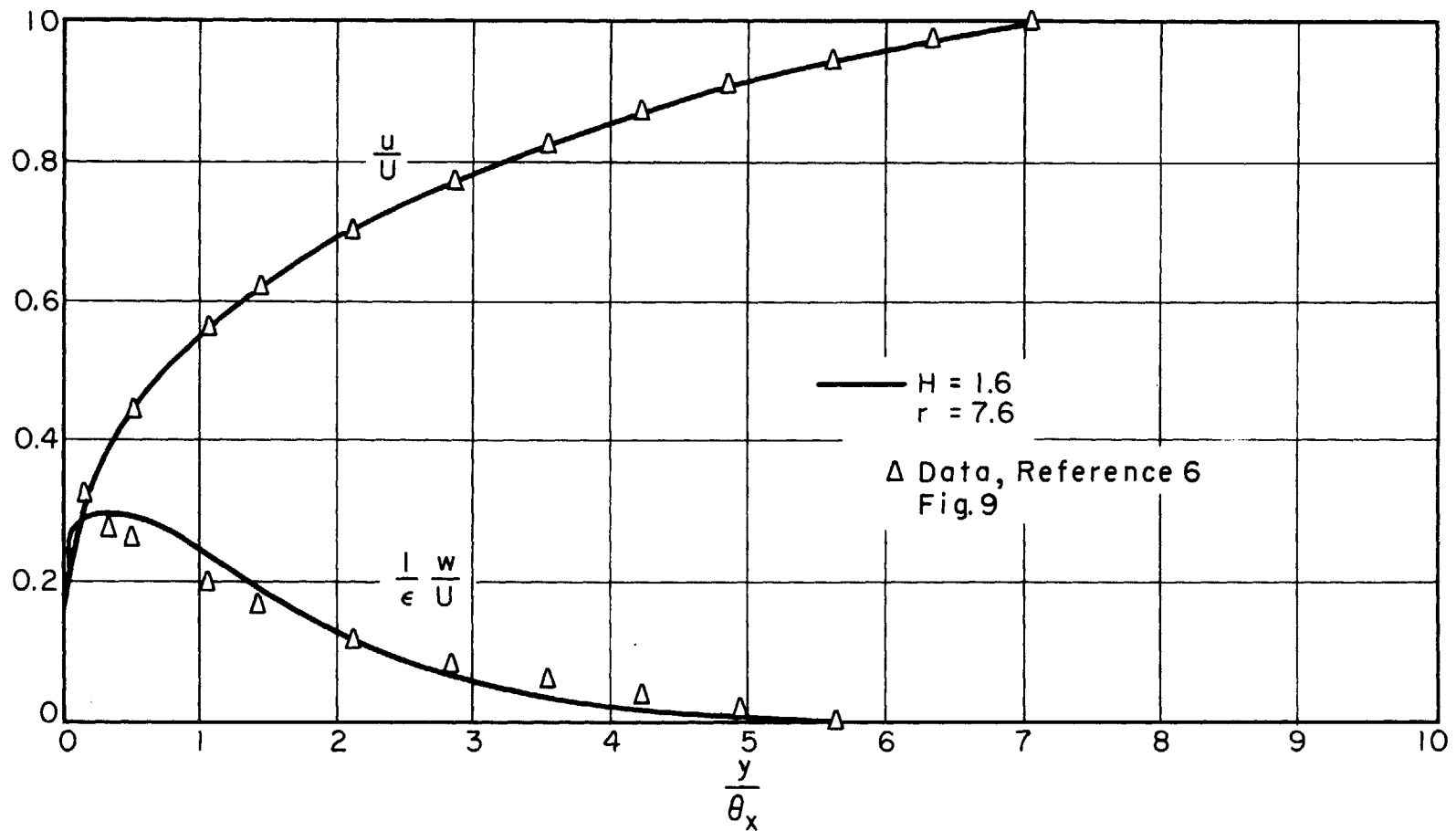


FIG. 23 - COMPARISON OF VELOCITY PROFILES ON THE BASIS OF H AND r WITH EXPERIMENTAL DATA FROM REFERENCE 6, FIGURE 9

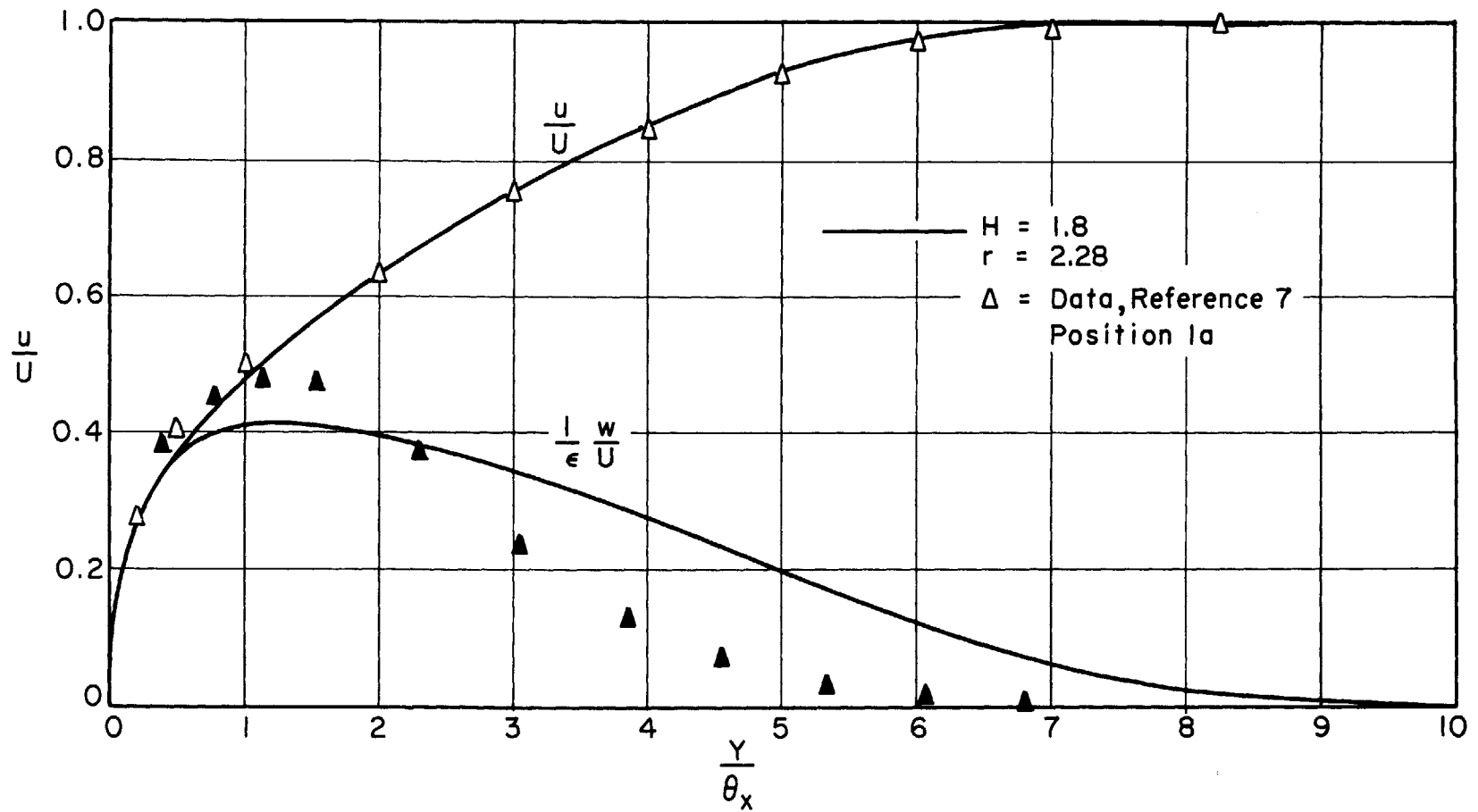


FIG. 24 — COMPARISON OF VELOCITY PROFILES ON THE BASIS OF H AND r WITH EXPERIMENTAL DATA FROM REFERENCE 7 POSITION 1a

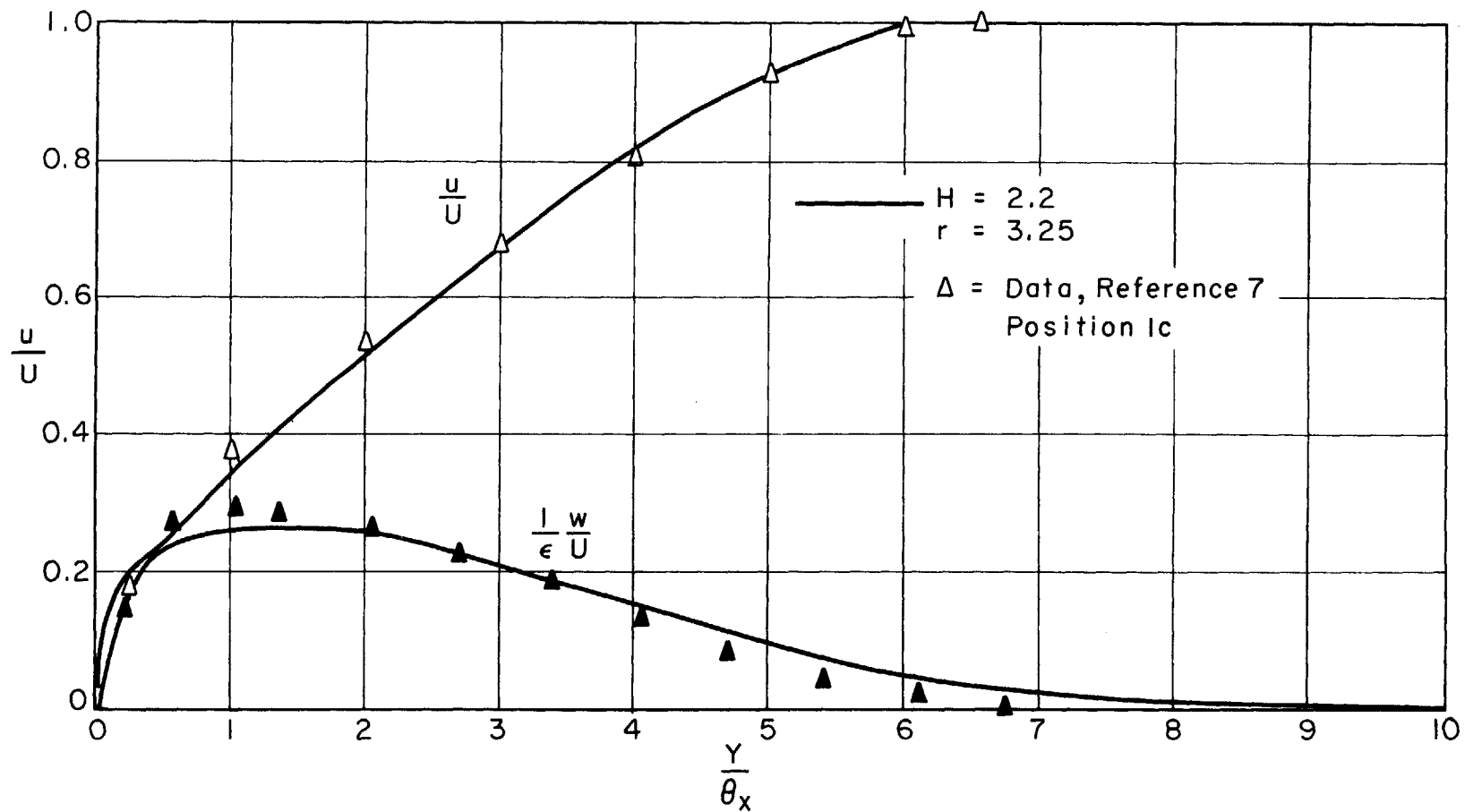
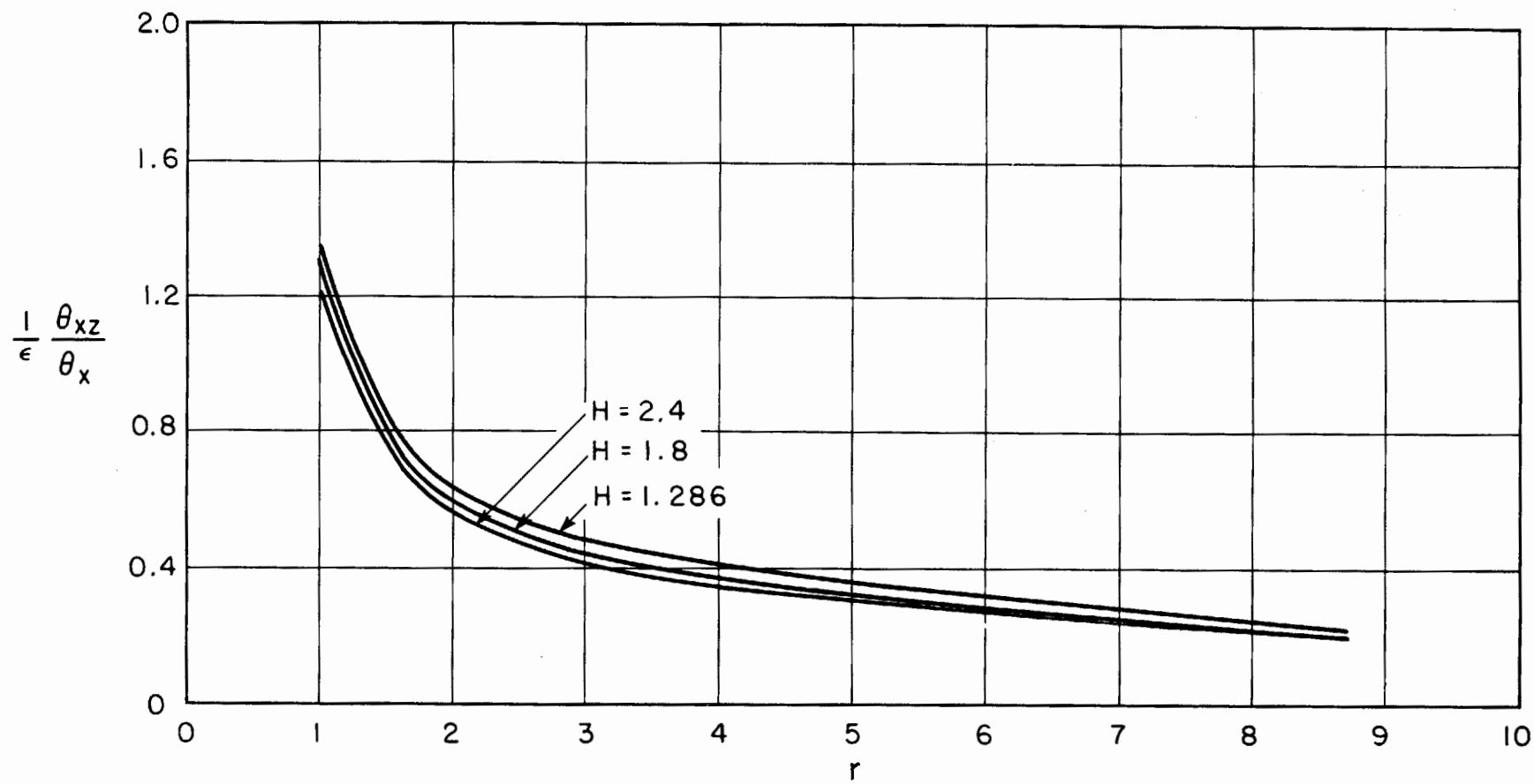
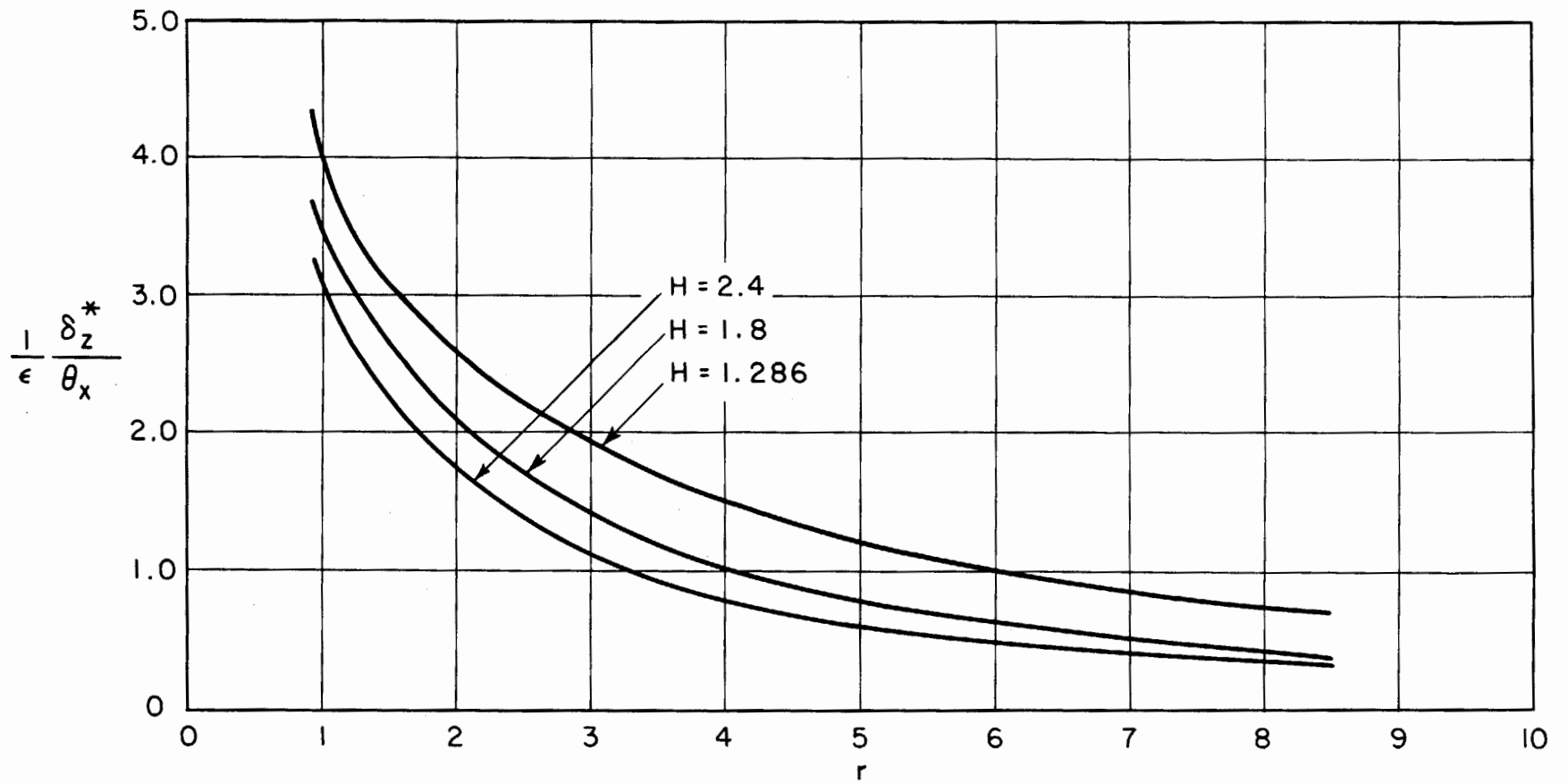


FIG. 25 - COMPARISON OF VELOCITY PROFILES ON THE BASIS OF H AND r WITH EXPERIMENTAL DATA FROM REFERENCE 7 POSITION 1c



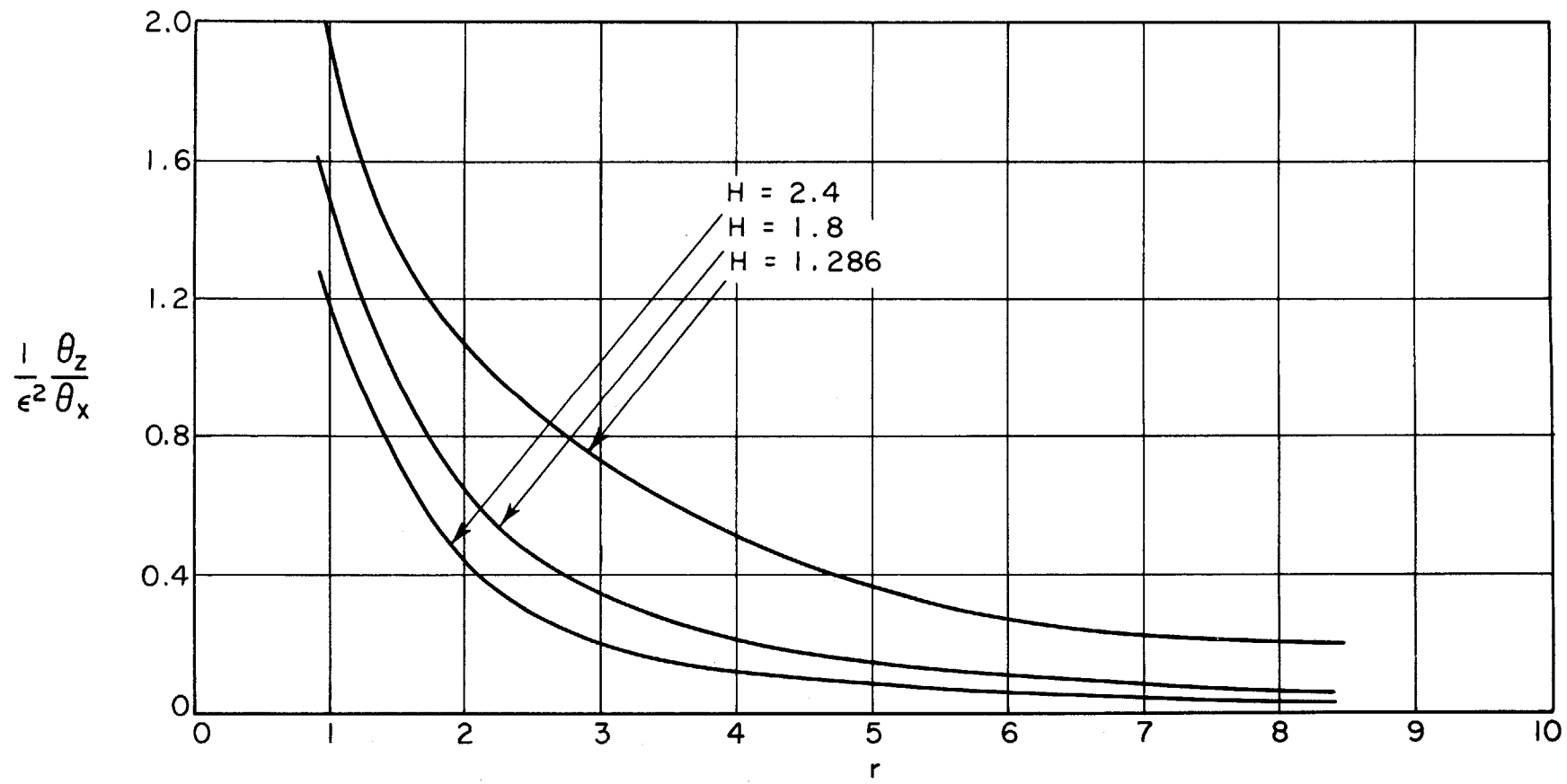
RELATIONSHIP BETWEEN $\frac{1}{\epsilon} \frac{\theta_{xz}}{\theta_x}$, H , AND r

FIGURE 26



RELATIONSHIP BETWEEN $\frac{1}{\epsilon} \frac{\delta_z^*}{\theta_x}$, H , AND r

FIGURE 27



RELATIONSHIP BETWEEN $\frac{1}{\epsilon^2} \frac{\theta_z}{\theta_x}$, H AND r

FIGURE 28

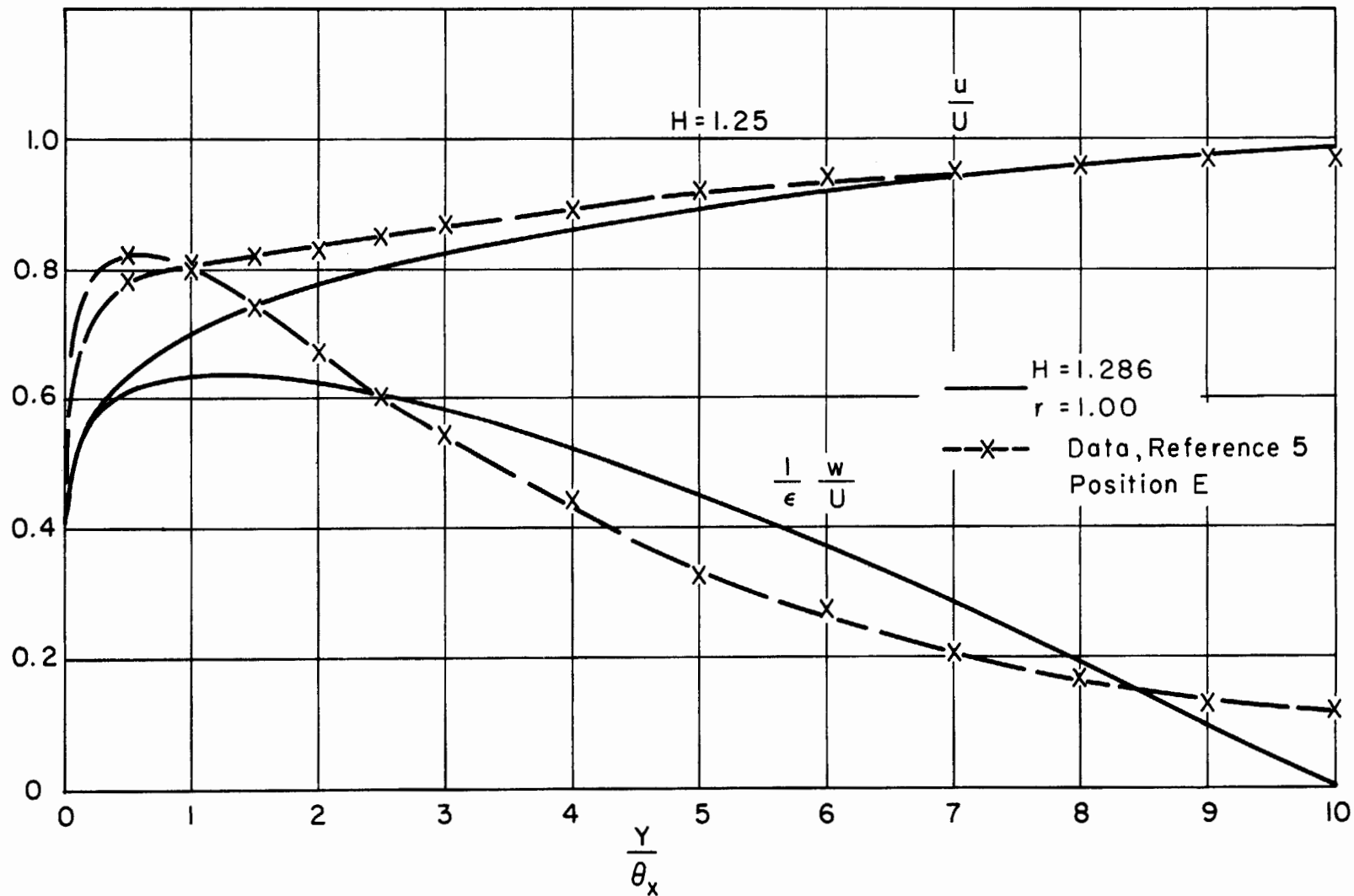


FIG. 29 COMPARISON OF VELOCITY PROFILES ON THE BASIS OF H AND r WITH EXPERIMENTAL DATA FROM REFERENCE 5.

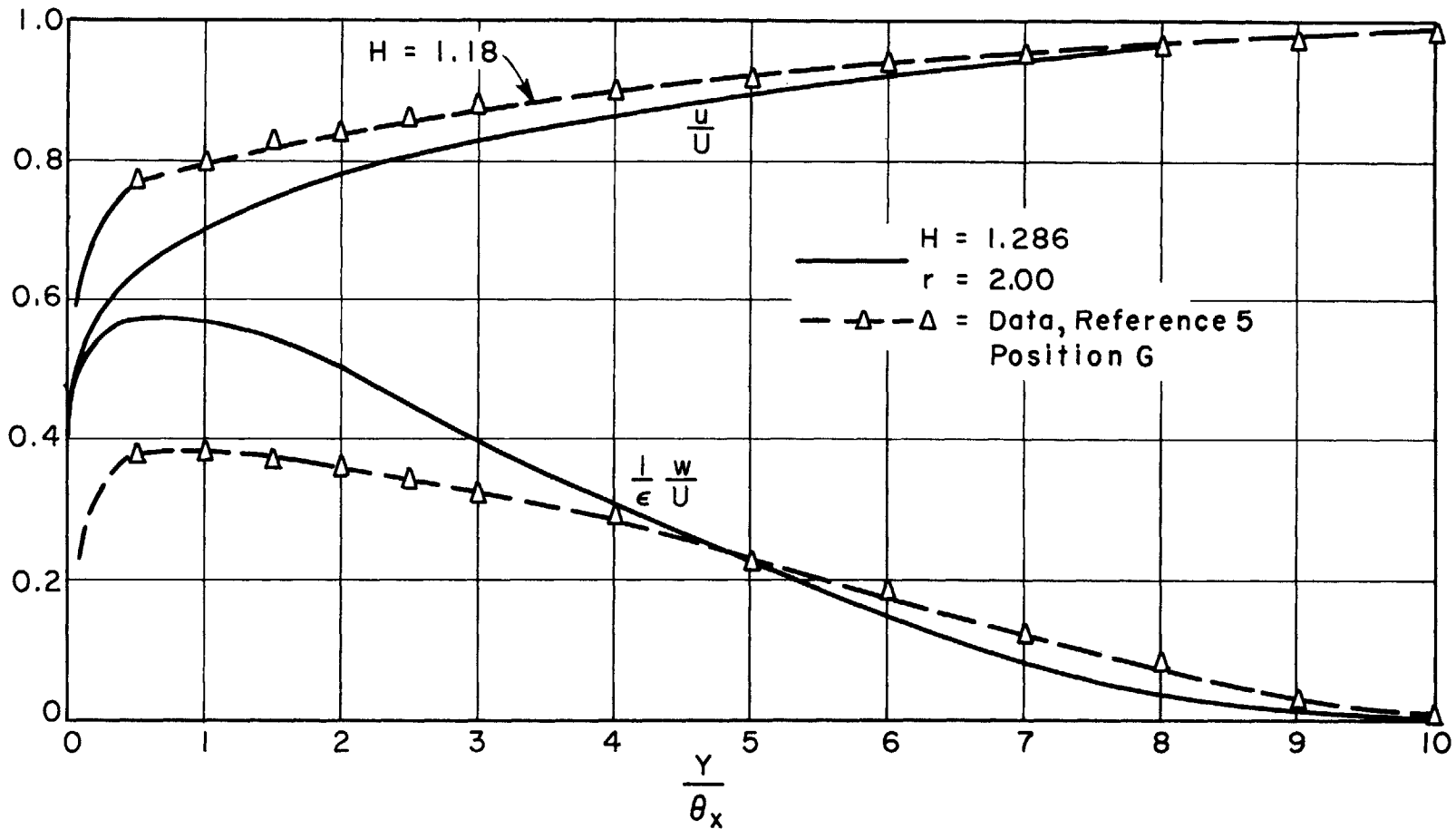


FIG. 30 - COMPARISON OF VELOCITY PROFILES ON THE BASIS OF H AND r WITH EXPERIMENTAL DATA FROM REFERENCE 5

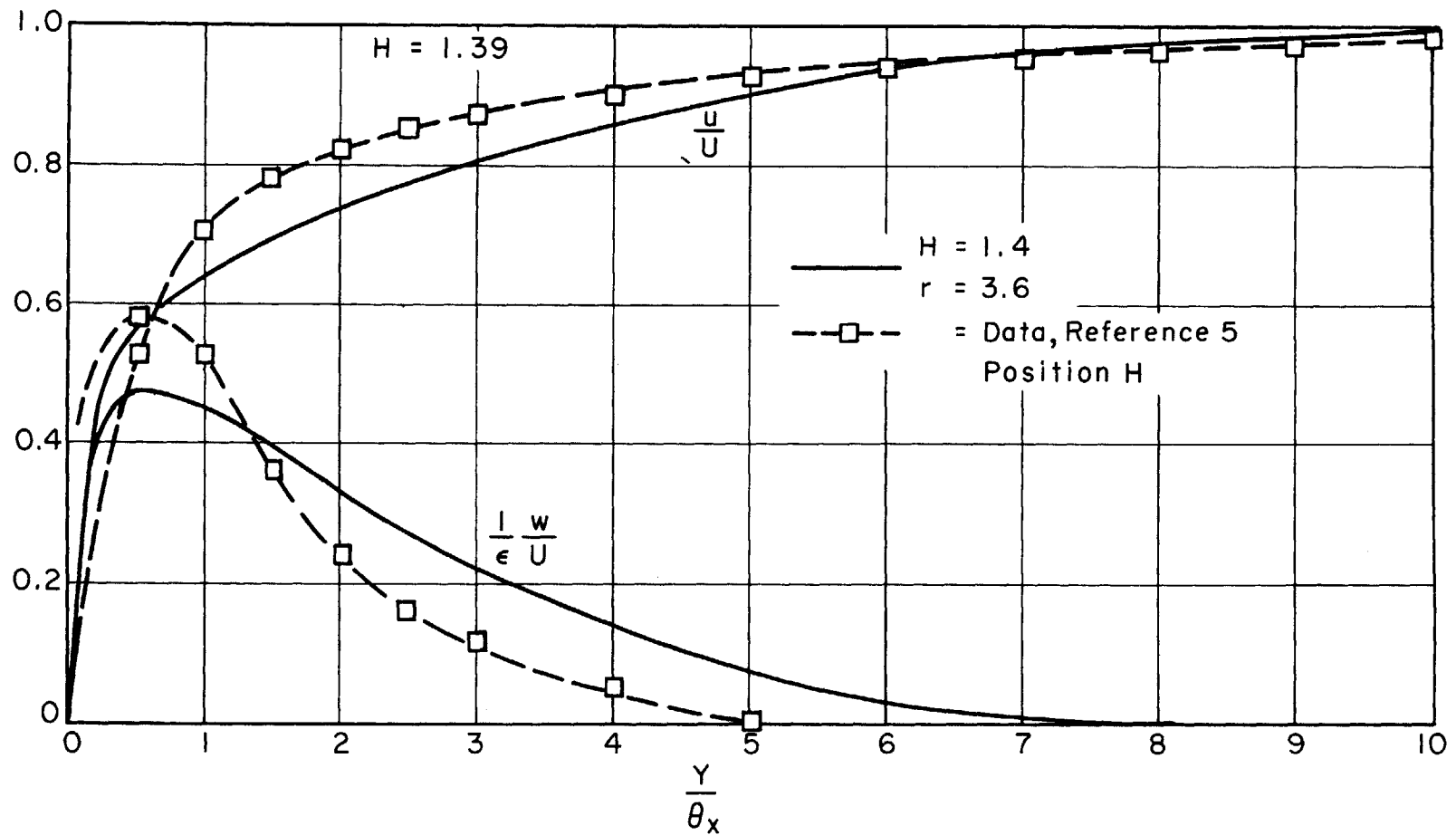


FIG. 31 - COMPARISON OF VELOCITY PROFILES ON THE BASIS OF H AND r WITH EXPERIMENTAL DATA FROM REFERENCE 5

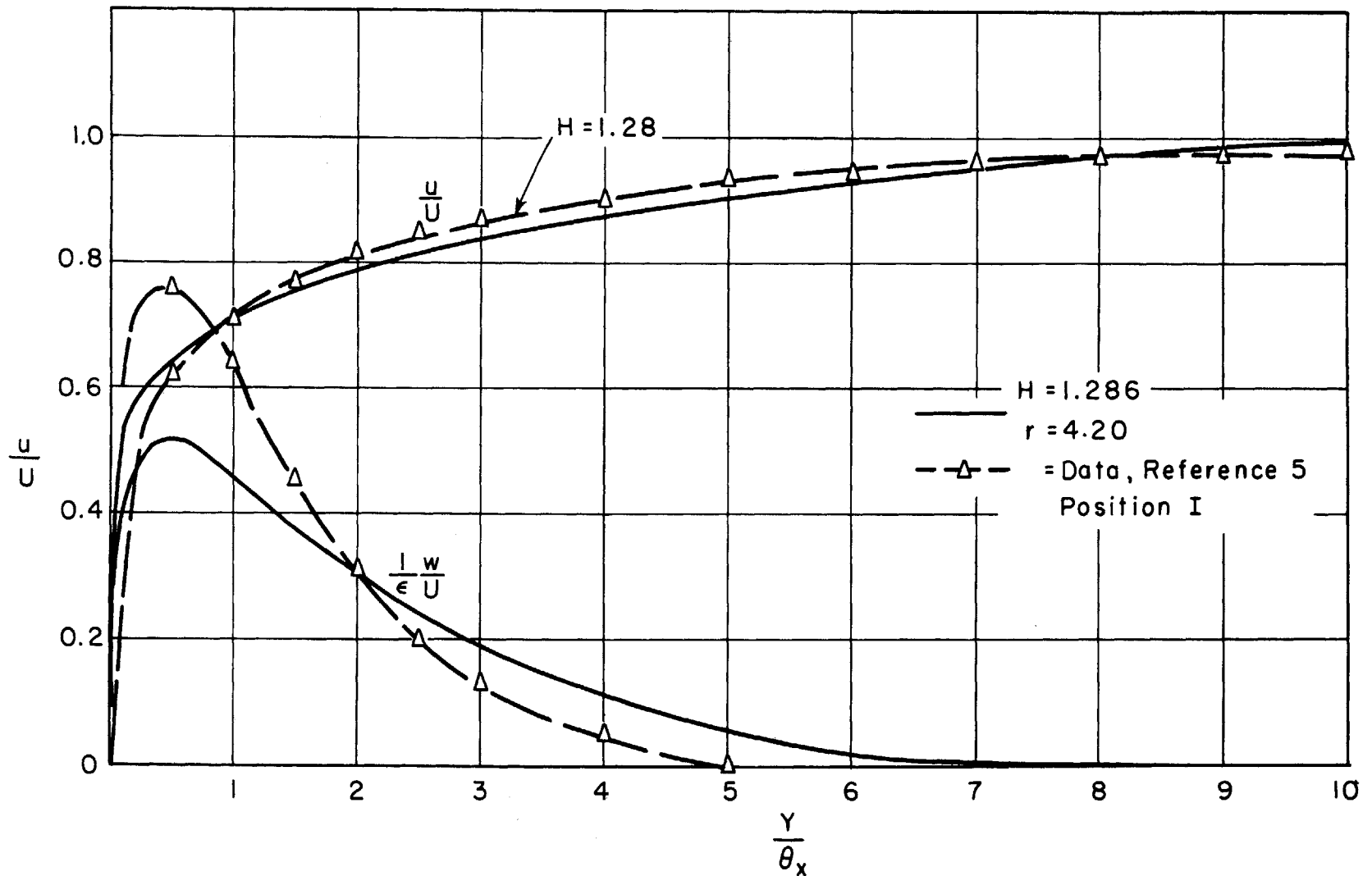


FIG. 32 COMPARISON OF VELOCITY PROFILES ON THE BASIS OF H and r WITH EXPERIMENTAL DATA FROM REFERENCE 5.

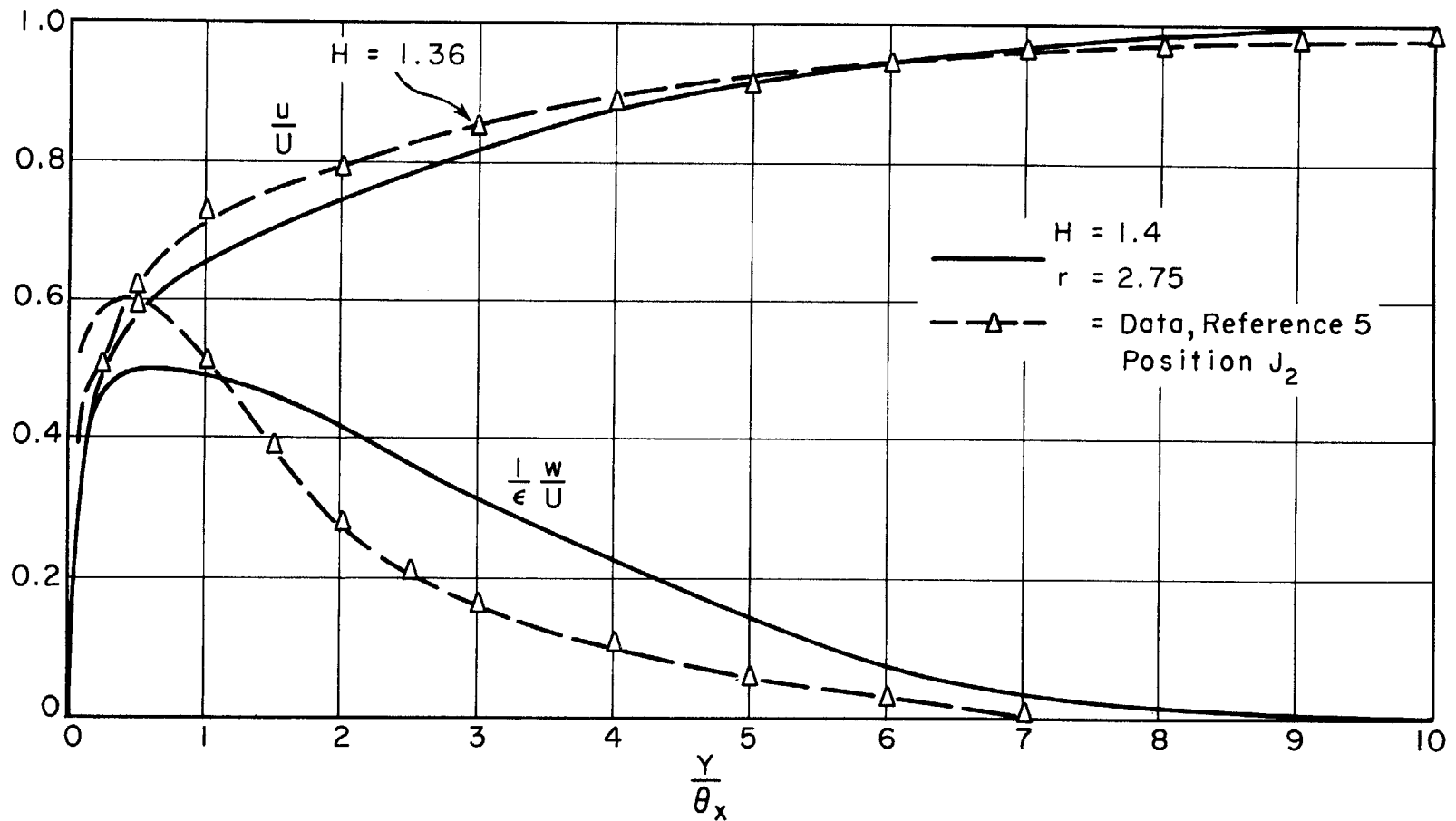
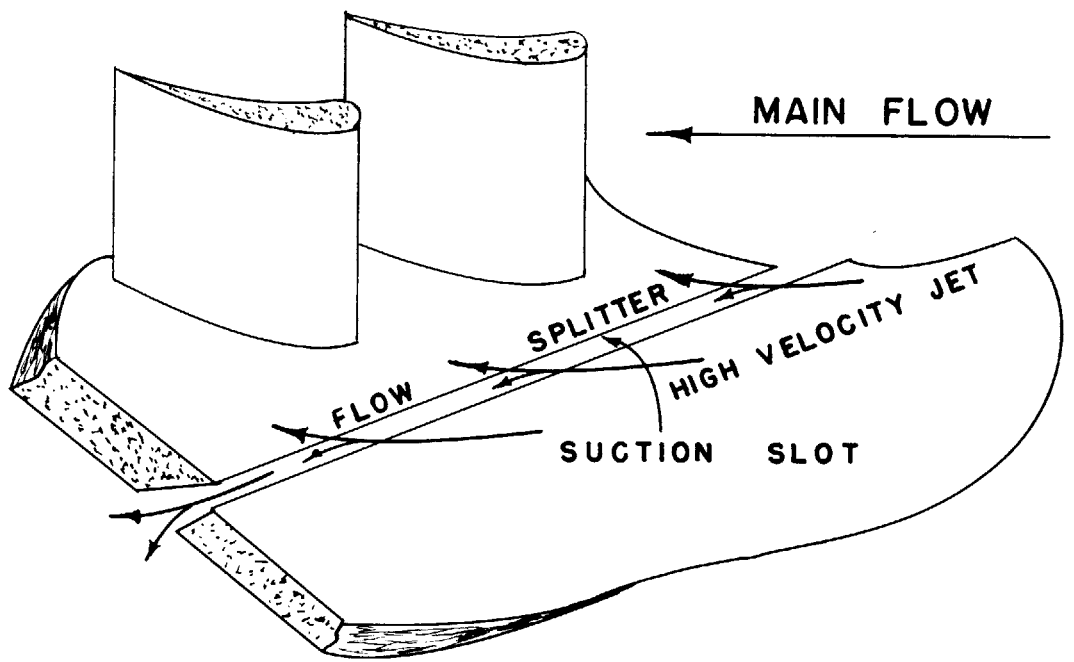


FIG. 33 - COMPARISON OF VELOCITY PROFILES ON THE BASIS OF H AND r WITH EXPERIMENTAL DATA FROM REFERENCE 5



FLOW SPLITTER AND SUCTION SLOT

FIGURE 34